6-23-2008

Modeling Recruitment/Derecruitment

Massa Christopher
University of Vermont

Follow this and additional works at: http://scholarworks.uvm.edu/graddis

MODELING RECRUITMENT/DERECRUITMENT
PHENOMENA IN THE INJURED MOUSE LUNG

A Thesis Presented

by

Christopher Barry Massa

to

The Faculty of the Graduate College

of

The University of Vermont

In Partial Fulfillment of the Requirements
for the Degree of Master of Science
Specializing in Biomedical Engineering

May, 2008

Accepted by the Faculty of the Graduate College, The University of Vermont, in partial fulfillment of the requirements for the degree of Master of Science, specializing in Biomedical Engineering.

Thesis Examination Committee:

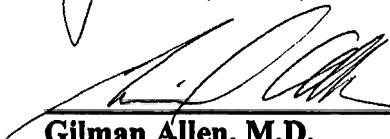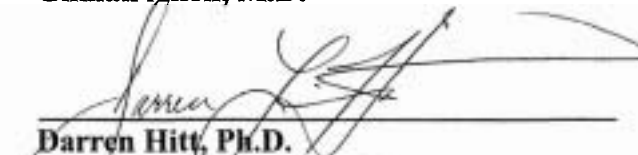_____ Advisor
Jason Bates, Ph.D., D.Sc.

_____
Gilman Allen, M.D.

_____
Darren Hitt, Ph.D.

_____ Chairperson
Fredric Sansoz, Ph.D.

_____ Vice President for Research
Frances E. Carr, Ph.D.   and Dean of Graduate Studies

Date: **March 20th, 2008**

ABSTRACT

Recruitment and derecruitment (R/D) of airways is known to significantly influence mechanical properties of the respiratory system during artificial ventilation, particularly in states of lung injury. The prevailing view of this phenomenon treats airway R/D as a static function of pressure. Recent experimental and clinical data suggests that this is not the case, but rather that R/D is an inherently dynamic process. In order to quantitatively assess the dynamics of lung recruitment during mechanical ventilation we extended a mathematical model by Bates and Irvin (9) for the purpose of fitting experimental data. The model of the lung consists of a parallel network of flow pathways with identical resistive and elastic elements. Each pathway is allowed to be either open, whereby it accumulates flow and decreases overall lung stiffness, or closed, increasing lung elastance and not participating in ventilation. The pathways are characterized by unique critical closing and opening pressures, and opening and closing velocities, each chosen from probability distribution functions. The rate of transition between an open and closed state depends on the magnitude difference between the pressure in the respiratory system and each unit's critical pressure times the airway's opening or closing velocity constant. Since the exact form of the pressure dependence governing recruitment and derecruitment remains unknown we explored four model variants to predict how opening or closing behavior is altered in injury.

The lung model was coupled with a computational model of a mechanical ventilator in order to simulate elastance changes following deep inflation (DI) at three levels of Positive End Expiratory Pressure (PEEP). Elastance measurements came from healthy or lung injured mice at 4, 14, 24 or 48 hours following intratracheal instillation of saline (control) or hydrochloric acid (injury). The Nelder and Mead simplex optimization method was used to minimize error between model variants and average experimental elastance for each condition. By comparing the residual error of the fits for each model, we have demonstrated that only one variant was able to recreate both the transient response to deep inflations and the response to static PEEP. In fitting the best model to data from individual mice we obtained estimates for parameters governing opening and closing behavior. Statistics and model sensitivity were determined for each parameter in every experimental condition. Comparison of parameter values between groups revealed a significant increase in closing and opening pressures from health to injury, which worsened with increasing injury severity. The progressive increase in critical pressures as injury worsens implicates surfactant deactivation as the likely cause of increased propensity for airway closing during acute lung injury.

Acknowledgements

TABLE OF CONTENTS

LIST OF FIGURES

LIST OF TABLES

Chapter 1   Introduction

During artificial ventilation, recruitment and derecruitment of small airways is known to contribute significantly to the mechanical properties of the respiratory system. Though derecruitment can be reduced by the application of positive end expiratory pressure (PEEP), the intrinsic propensity for airway collapse is exacerbated during acute lung injury (ALI). The prevailing scientific viewpoint treats recruitment as a static function of pressure; however, recent experimental data demonstrates that recovery of lung function following deep inflation is transient, and that dynamic peripheral airway recollapse becomes more rapid and profound as lung injury matures (5). It is known that the lung can tolerate periodic deep inflations – or recruitment maneuvers - to reopen collapsed lung regions, but that continued volleys of large breaths are injurious and significantly exacerbate the pathology. Clinically, physicians struggle in an attempt to balance the impact of these phenomena. The current convention is to ventilate at low tidal volumes over a moderate level of PEEP. Some clinicians have tried interspersing recruitment maneuvers in an *ad hoc* fashion, often without much efficacy.

We believe the lack of clinical efficacy in the use of recruitment maneuvers results in part from the lack of appreciation for the inherent dynamic nature of this process. In light of the clinical and experimental evidence indicating that the dynamics of airway R/D are fundamentally altered in the injured lung, we argue that the question surrounding the use of recruitment maneuvers is not whether they should be used, but rather when and how often they should be employed. It is thus therapeutically important to determine how deep inflations should be given in order to optimize the state of recruitment in the injured lung. In order to achieve such a goal, a quantitative

understanding of the dynamics of recruitment and derecruitment phenomena is essential. At present, there exists no quantification of the distribution of pressures and rates governing airway opening and closing behavior. Characterization of these distributions – in particular of how they evolve as injury matures - is essential to the development of an effective recruitment strategy that maintains respiratory function at minimal stresses to the lung.

In order to determine how the distributions of these rates and pressures determine mechanical function in health and disease, we designed a novel computational model to be fit to experimental data. We began by extending the dynamic R/D paradigm by Bates and Irvin (9) by altering the mechanics and structure of the model and coupling it with a simulated mechanical ventilator. Once this implementation of the lung-ventilator system was validated, we simulated the time course of experiments measuring the stiffness of mouse lungs following deep inflation at three levels of PEEP. By fitting several proposed models to experimental data from healthy and lung injured mice at various times following intracheal acid-instillation we have identified one model as paramount in characterizing the data. Using the best model, we have estimated values for parameters governing opening and closing behavior in the experimental data. Analysis of parameter values indicates that airways in the injured lung require greater pressures to open them and will close at higher pressures than in the healthy lung. Comparison of these results with the literature suggests that the mechanism by which dynamic collapse is exacerbated during acid induced lung injury is primarily through the inactivation of pulmonary surfactants.

Chapter 2   Background

2.1   Respiratory Anatomy and the Physiology of Breathing

Respiratory function is essential for the maintenance of homeostasis, with cessation of ventilation uniformly resulting in tissue ischemia, eventually progressing to irreversible organ damage and death if untreated. The most evident, and indeed the most important function of the respiratory system is to allow the exchange of soluble gasses between the air and the blood. In one minute the lungs filter the entirety of the body's blood volume, normally ensuring adequate delivery of oxygen to the blood and elimination of carbon dioxide.

In order for the respiratory system to succeed in these functions, air must undergo bulk transport from the outside of the body to a surface designed for interfacial exchange of soluble gasses. The primary driving force for bulk motion of gas is contraction of the diaphragm, a large muscle beneath the lungs that is under control by the autonomic nervous system. When the diaphragm contracts the chest cavity expands downward into the abdomen, producing a negative pressure across the chest wall. Air is then sucked through the mouth and nose into the oropharynx and into the trachea, where it enters the lung. The lung is composed of a branching network of tubes, called airways, which are embedded in lung tissue, called parenchyma. As the distance from the trachea increases, the airways decrease in size and cartilage content. Beyond a certain distance from the trachea, the airways begin to have specialized structures for gas exchange called alveoli. The presence of alveoli becomes more frequent further down the airway tree, eventually terminating in a cluster of alveoli called an acinus. Airflow is divided down the airways until the gas reaches these acini, where the majority of gas exchange occurs passively by

diffusion. Exhalation occurs when the muscles of the respiratory system relax and gas is forced from the respiratory system by the elastic recoil of the lung parenchyma and chest wall. The pressure remaining at the end of exhalation when the subsequent inspiration begins is referred to as the end expiratory pressure.

2.2   Models of Respiratory Mechanics

The mechanical properties of the airways and parenchymal tissues are significant determinants of the work of breathing and ultimate distribution of ventilation in the healthy and diseased lung. In the most basic model of respiratory mechanics, the lung is simplified to act like a linearly resistive pipe in series with an elastic element that accumulates flow, while the volume, flow and pressure are, in general, functions of time, t. In this "single compartment" model (Figure 1. A), airway pulmonary pressure, P_{aw}, is equal to the sum of contributions of flow through the resistive tube, $\dot{V}_L$, and the recoil caused by volume, V_L, distending the elastic component

$$P_{aw}(t) = R_L \dot{V}_L(t) + E_L V_L(t) + P_0 \tag{1}$$

where P_o is the equilibrium pressure of the respiratory system within the chest wall, R_L is the apparent lung resistance and E_L is the apparent lung stiffness. In this model changes to the contribution of resistance are typically interpreted as alterations in the caliber of the airways, while elastance changes are typically viewed as stiffening or softening of the parenchyma. This model provides no insight into the mechanism by which these changes occur, nor does it provide any anatomic insight into localizing these alterations. This model is often efficacious in time-domain characterization of respiratory mechanics, but it suffers the inability to separate the contributions of airway wall distension from

parenchymal elastance, or thermal losses due to internal resistance of parenchymal tissues from airway resistance.

Figure 1: Simple models of the respiratory system.
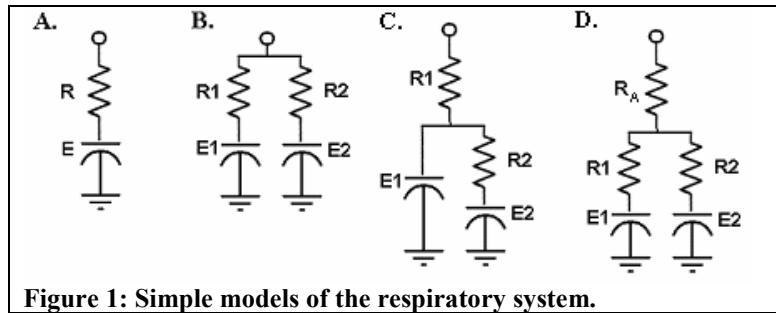
Additionally, this model neglects the frequency dependant effects arising from the inertia of accelerating gasses and the complex viscoelastic rheology of biologic materials.

Several simple models have been proposed to minimize the impact of these shortcomings. In 1956 Otis (49) proposed a model (Figure 1. B) with two resistive-elastic pathways in parallel with the compartments having different time constants. This model allowed for ventilation distribution heterogeneity and imparted slightly improved frequency dependence. Still, the lack of anatomic fidelity precludes its utility in localizing pathology. A common central airway resistance may be added (Figure 1.D), however this introduces another free parameter without allowing for more poignant inferences to be made. Another partitioning of mechanics can be achieved by representing the central airways as one resistance, with airway wall compliance in parallel to a resistive-elastic peripheral lung component (Figure 1. C). In this model, the distension of airways and the resistance of the periphery are explicitly partitioned, allowing for further insight in certain pathologies, particularly emphysema and chronic obstructive pulmonary disease (42, 59).

Parameter estimation in the frequency domain frequently employs a four parameter model which reliably characterizes the mechanics of the mammalian lung below 30 Hz (34). The linear airway resistance to flow, R, is placed in series with a

5

frequency dependant inertial term, *I*, and a viscoelastic tissue element, representing the

acinar compartment. Mechanics of the lung periphery are modeled by using "constant

phase" viscoelastic tissue properties with impedance, Z_{ti},

$$Z_{ti} = \frac{H(\eta - j)}{\omega^\alpha}$$

Figure 2: Schematic representations of Weibel and Horsfield's models of the lung.
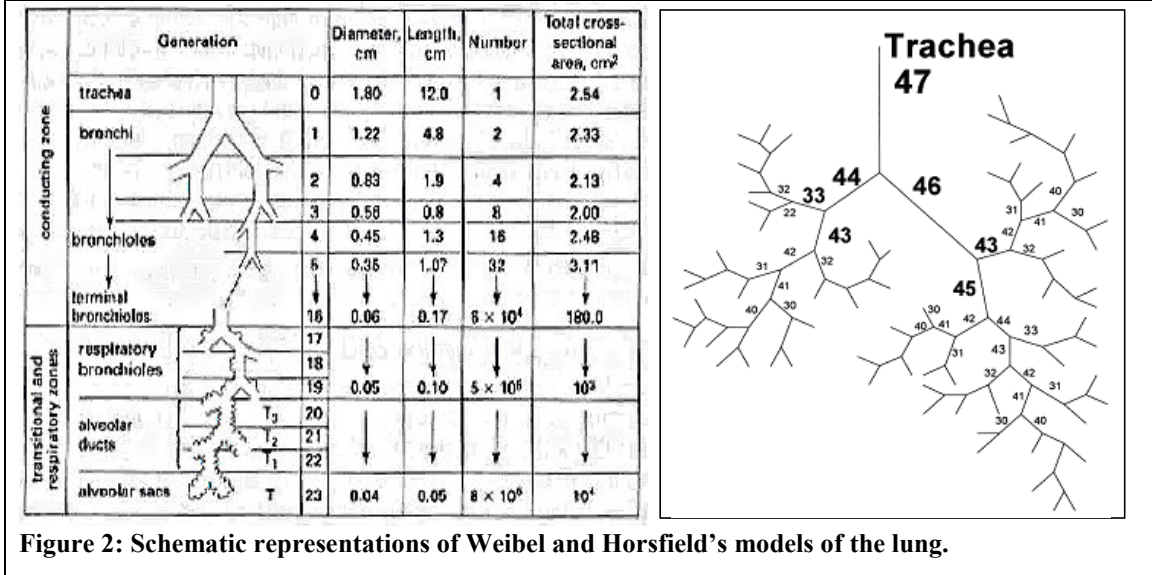
where *j* is the unit imaginary number, ω is the angular frequency, *H* is the tissue stiffness,

η is tissue hysteresivity (defined as the ratio of viscous dampening to elastic storage) and

$$\alpha = \frac{2}{\pi} \tan^{-1}\left(\frac{1}{\eta}\right). \tag{2}$$

This tissue element contributes a hyperbolically decaying component to both the real and

imaginary parts of the lung impedance with the element's phase being frequency

invariant. This model has the impedance

$$Z_L = R + j\omega I + \frac{H(\eta - j)}{\omega^\alpha} \tag{3}$$

and is adequate to characterize the function of the lung during health and mild illness; however, severe disease – especially when regional mechanical properties are heterogeneous – diminishes its reliability and accuracy (40). Several investigators have adapted this model to accommodate for heterogeneity in airway and tissue properties, estimating distributions of parameters in various diseases (38, 39, 41, 59).

Incorporating airway collapse and reopening into a lung model requires a distribution of mechanical elements whose properties depend on their state of recruitment. The simplest implementation of R/D processes allows for airways to exist in one of two binary states - open, whereby it participates in ventilation, and closed, where it does not – and a relationship specifying the conditions sufficient and necessary to transition between each state. The simplest and the most well accepted transition condition was formalized by Hickling (36), whereby each airway is assigned both a threshold opening pressure (TOP), above which airways will have a volume determined by the applied airway pressure, and a threshold closing pressure (TCP), below which airways will have zero volume. Simulation using distributions of TOP and TCP allowed the model to recreate the Pressure-Volume relationship of the lung, as well as its response to PEEP (36). The utility of this model in predicting an ideal level of PEEP was examined, but found unreliable, as the slope of the P-V curve is highly variable near the lower inflection point of the curve (35). Additionally, the model fails to take account for the impact of volume history, which is known to exert time-dependant effects on mechanics through transient recruitment.

In order to overcome these limitations posed by Hickling's static recruitment model, Bates and Irvin (9) added a dynamic element to the process of recruitment and

7

derecruitment. In this model, airway transition between binary states is not instantaneous upon crossing over the threshold pressure. Instead, each airway approaches a transition between states with a rate proportional to the difference between the threshold pressure and the pressure delivered to the airway. Proportionality constants relating the applied pressure gradient to the rate of transition between states are pulled from probability distribution functions for each airway. This effectively imparts a pressure dependent delay to the process of transition between open and closed states that varies between airways, allowing for natural variation in the timing and pressure dependence of airway collapse. This model was shown capable of recreating the progressive lung stiffness increase that occurs during mechanical ventilation solely using stochastic collapse.

Morphometerically accurate anatomic models allow for the highest level of resolution, however they are generally implemented in the frequency domain as this greatly simplifies the governing equations. Two commonly referenced characterizations of mammalian lungs that were developed from anatomic plaster casts are Weibel's symmetrically branching model (64) and Horsfield's asymmetric model (37) which uses recursion relations to impose self similarity in the airway tree (Figure 2). This degree of complexity allows very reliable forward simulation, but direct parameter estimation becomes incredibly arduous due to the number of degrees of freedom imposable upon such model architecture. Constant phase model parameters may however be obtained by fitting to the impedance spectra of the above anatomic models. Airway segments are given impedances based on their geometry, with radius and length determining resistance through Pouiselle's law and intertance through segment volume and gas density. The division of flow down the airway tree depends on the mechanical impedance of the

8

subtended airway network. Some flow may not be transmitted through to the subtending airways as distension of airway walls or compression of gas act as parallel pathways by which flow can be lost. By changing the distribution of airway and tissue mechanics various pathologies may be simulated, and inferences may be drawn regarding the distribution of ventilation, work of breathing and extent of flow losses due to airway distension.

2.3   Pathophysiology of Acute Lung Injury

Acute lung injury (ALI) is a significant factor affecting morbidity and mortality in the intensive care unit (62). ALI may result from pulmonary disease (eg. pneumonia), complications of extrapulmonary illness (eg. sepsis, pancreatitis) or traumatic injury (29, 51). Patients with ALI have impaired gas exchange, alveolar flooding and increased lung stiffness due to obstruction or collapse of small airways. Patchy opacities can be seen on a chest x-ray, indicating a diffuse rather than homogenous pathological process (18, 63). Since the 1960s, clinical management of the patient with ALI has entailed endotracheal intubation and artificial mechanical ventilation. Mechanical ventilation is essential to support life in many critically ill patients; however, the generation of high pressures or large volumes may actually cause or exacerbate lung injury.

Though a plethora of novel strategies have been proposed for use in safely ventilating patients, the mortality associated with ALI remains between 40 and 60% in most epidemiologic studies, virtually unchanged since its initial characterization (63). One of the few interventions demonstrated efficacious in improving patient outcome is the introduction of low tidal volume ventilation with moderate Positive End Expiratory

Pressure (PEEP), which is believed to reduce injurious stresses to the lung (1, 12, 20, 60-62). This strategy succeeds by minimizing both over-distension of the parenchyma and airway collapse by ventilating with small breaths while supporting airway opening with static pressure during exhalation.

An adjunct to this approach that is presently employed by some clinicians is the sporadic application of a larger breath, or recruitment maneuver, which generates higher airway pressures that reopen collapsed regions of the lung. These recruitment maneuvers have been used to transiently improve gas exchange and mechanical function of the lung, though clinically significant responses have been observed nearly exclusively in the early stages of ALI when elastance increases are primarily due to derecruitment, as opposed to changes to the intrinsic tissue properties that appear to occur in late ALI (32, 61, 62). The recruiting of potential flow pathways allows for a fixed tidal volume to distribute more evenly throughout the lung, which in turn generates lower airway pressures. Over time, some airways will derecruit, causing progressive increases in lung stiffness, maldistribution of tidal volume and increased injurious stresses to the lung. At present, debate exists whether the application of recruitment maneuvers truly results in reduction of injury or if the large breaths generate high shear stresses and serve to potentate injury; in practice this distinction is likely dependent on disease etiology and injury severity.

A major reason for the controversy surrounding the delivery of recruitment maneuvers stems from a fundamental misunderstanding of the way airways recruit and derecruit. The prevalent viewpoint among most clinicians and respiratory physiologists treats the amount of recruited lung as a static function of pressure. In this description of recruitment, lung units open instantaneously once a certain critical pressure is applied to

an airway; similarly the airway closes immediately once its pressure falls below the critical pressure. In truth, airway opening is a dynamic process which requires propagation of a gas plug in a fluid filled tube until the Marangoni stresses that stabilize the air-liquid interface are overcome (10). Similarly, airway collapse has inherent dynamics associated with surfactant driven flows that reform fluid menisci, called liquid bridges, within the airway lumen. At present, factors governing these dynamic processes are poorly understood.

2.4   Biophysics of Airway Recruitment and Derecruitment

The dynamic nature of airway R/D is not simply a theoretical concern and has been observed experimentally *in vivo* and *in vitro*, as well as in mechanically ventilated patients. Modeling studies have attempted to discern what biophysical processes underlie airway recruitment and derecruitment phenomena, as well as to identify how this process is altered by and contributes to lung injury. Whether an airway collapses upon itself or simply floods while maintaining its geometry may affect the dynamics of reopening (66). Airways that are simply flooded require a disruption to the meniscus of the fluid plugging their lumen, while airways that collapse may be folded upon themselves and destabilized, requiring a peeling apart of their walls (52, 53, 66). Debate as to which of these mechanisms is prevalent in acute lung injury has yet to be resolved. In either case, airways have been observed to open sequentially down the tree at varying distending pressures, presumably as a function of geometry and the tethering forces exerted by parenchyma (30, 31, 52, 53, 55, 56, 58). Both experimental and theoretical studies have attempted to separate the threshold pressures for transition between opening and closing

from the impact of pressure on the rates of these processes. Methodologic constraints have complicated the separation of these effects at length scales ranging from the single airway to the system level.

Studies in the excised lung have granted insight to the global behavior demonstrated by reinflation under various mechanical conditions. In a study of dynamic air trapping during ventilation, Frazer et. al. inflated previously degassed rat lungs at various rates and observed that lower flow rates and lower peak pressures lead to increased trapped ventilation, independent of the peak pressure reached (26). Subsequently, Frazer examined changes to the rat pressure-volume curve at various end-expiratory pressures to demonstrate that 68% of rat airways are occluded by formation of menisci at pressures between 1.4 and 3.0 cmH$_2$O (25). In the face of pulmonary edema, menisci were demonstrated to form at higher transpulmonary pressures, indicating that the wet, injured lung is more prone to small airway and alveolar collapse (24). These menisci were originally suggested to be foam-like in nature and exist at the level of the alveoli or small airways (27). It was later demonstrated menisci may form at varying generations in the airway tree and form sequential obstructions to the delivery of gas to the lung periphery.

The concept of sequential blockages was extended to explain the discrete nature of lung resistance changes during reinflation, whereby the size and time intervals between these discrete changes appears to be distributed according to power-law distributions, reminiscent to the "avalanching" behavior seen in self-organized, critical systems (58). Upon reinflation of excised rabbit lungs, airways less than 2 mm in diameter showed a wide distribution of critical opening pressures; however, when

12

lavaged with surfactant the distribution of threshold pressures became markedly more narrowed, and the avalanching behavior was fully ablated (57). Modeling of this phenomenon in a symmetrically branching airway tree revealed significant variation in the initial airway generation where blockages begin to occur, as well as a considerably higher threshold for subtree opening (23+/-4 cmH$_2$O) (57). Experiments in reinflating the excised dog lung have shown power law distributions of discrete lung elastance changes which were similarly predicted by a model of avalanching reopening (56). These discrete avalanches in mechanical function were correlated with acoustic evidence of airway reopening in several studies (16, 23, 55).

Bench-top experiments performed in artificial airway-like systems subject to various fluid mechanical conditions have given insight to the biophysics that governs collapse at the level of the airway. In fluid lined tubes supported by axial tension the relative importance of viscous and surfactant effects has been linked to the capillary number

$$Ca = \frac{\mu v}{\gamma} \tag{4}$$

where μ is the fluid viscosity, v is the fluid velocity and γ is the surface tension of the lining fluid (31). In this study threshold opening pressure was noted to increase with increases in μ and γ, while it decreased with increases in axial tension and airway radius. For values of $Ca < 0.5$ the empirical relationship for opening pressure

$$Po = 8.3\frac{\gamma}{r} \tag{5}$$

was derived from the experimental data, where r is the radius. For higher capillary numbers, viscous forces generated threshold opening pressures higher than those

13

predicted above. The relevance of the empirical relationship to airways, as well as the validity of the model system, was confirmed by comparing the predicted threshold opening pressures to data obtained by direct visualization of reopening using air bronchograms (45). The value for surface tension was estimated near 35 dyn/cm, supporting the notion that surfactant facilitates the reopening of closed airways and is essential for stability of the airway tree (45). Subsequent studies in collapsed tubes with no axial tethering had similar yield pressures as those predicted above; however, the rates of airway reopening were noted to rise with increases in fluid viscosity (52). When outward tethering forces were added to the benchtop model (53) the airway patency, Γ, was related to the pressure differential across the air-liquid interface:

$$\Gamma = \frac{\nabla P}{\gamma/r}. \tag{6}$$

Analysis of the predicted and observed airway reopening pressures during bubble propagation in elastic tubes indicates that airway walls are subjected to very high shear stresses during reopening conditions (30). Subsequent experiments that exposed cultured cells to a moving air-liquid interface implicate steep normal pressure gradients at the bubble front as the likely cause of epithelial cell injury; administration of additional surfactant to this system was shown to completely ablate cellular injury (11). The extent of injury was found curiously independent of the duration of exposure to an isolated pressure gradient; however, pressure gradients that were sub-injurious if given once resulted in cumulative injury upon repeated exposure (43). Halpern and Grotberg studied the effects of surfactant on the stability of fluid lined tubes, concluding that a critical film thickness, ε_c, exists above which liquid bridges spontaneously form due to gradients in

surfactant concentration (33).   The value of ε_c was shown to decrease with increased

surface tension and wall compliance, while the administration of surfactant was shown to

reduce ε_c by 60% and to decrease the rate of collapse by a factor of five (33).

A series of experiments in living animals has demonstrated that lung mechanical

function in healthy and lung injured rodents is transiently recoverable following a deep

inflation, implicating collapse as the predominant cause for increased lung stiffness

during artificial mechanical ventilation.. In saline lavage injured mice, initial reopening

immediately following deep inflation was impaired, followed by a significantly hastened

and much more extensive increase in airway collapse (4). Rats receiving high volume

ventilation had more profound regional collapse than those receiving low volume

ventilation with sporadic deep inflation as assessed by increasing lung stiffness and large

uninflated regions of parenchyma on *in-vitro* microscopy (6). Additionally, the lungs of

mice receiving low volume ventilation were more persistently recruitable than those

getting high volume ventilation only (6). In a subsequent study, mice receiving low

volume ventilation with sporadic recruitment maneuvers had the lowest levels of

biomarkers for lung injury severity, out performing high volume ventilation and low

volume ventilation without recruitment maneuvers (7). More recently, Allen et al found

that recruitment after a deep inflation became progressively impaired over 48 hours

following intratracheal hydrochloric acid instillation (5). These studies suggest that the

dynamics of recruitment and derecruitment are of significant concern in experimentally

induced lung injury and that the beneficial response to recruitment maneuvers is

diminished as pulmonary dysfunction worsens.

Chapter 3   Methods

3.1   Modeling Recruitment / Derecruitment in a Single Airway

Our model of recruitment and derecruitment of an individual lung unit was adapted from the model developed by Bates and Irvin (9). In the original model, a lung unit consists of a resistance-less, collapsible airway subtending an alveolar compartment. The airway exists in one of two states, either fully open or fully closed. When the airway is open the alveolar compartment volume is determined by the airway pressure, P_{aw}, according to the Salazar-Knowles pressure-volume relationship (54),

$$V = A - Be^{-KP_{aw}} \tag{7}$$

where A, B and K are empirically determined constants. If the airway is closed, the compartment volume is equal to zero. Whether an airway is open (recruited) or closed (derecruited) depends on its volume history represented by its position on a virtual trajectory. The virtual trajectory is a formalization of the delay arising from the dynamics of dissolution or formation of fluid menisci that obstruct the airway and prohibit it from partaking in ventilation. An airway's position, x, on this trajectory is allowed to vary on the range of 0 to 1, with the endpoints corresponding to the threshold for transition to the closed and open state respectively. More explicitly, an airway moves along the virtual trajectory by changing its value of x without any perceptible impact on mechanics until it reaches the boundary for transition into the opposite state. If an airway is open, it will close only when its value of x reaches 0, otherwise it remains open; similarly, the closed airway will only open when the x value reaches 1. This behavior is reminiscent of the nonlinear Schmitt Trigger circuit element, which is used to generate hysteresis and impart stability where a comparator would normally be used.

16

The dynamics by which an airway moves on this trajectory depend on the applied pressure and the values of three parameters: a critical pressure, P_{crit}, an opening velocity, S_o, and a closing velocity, S_c. Movement along the virtual trajectory is governed by a piecewise-linear first order differential equation

$$\frac{dx(t)}{dt} = \begin{cases} s_o(P_{aw} - P_{crit}) & P_{aw} > P_{crit} \\ s_c(P_{aw} - P_{crit}) & P_{aw} < P_{crit} \end{cases} \tag{8}$$

where P_{aw} is the pressure delivered to an airway. Lung units receiving pressures above their critical opening pressure will thus move closer to opening with a rate directly proportional to the pressure differential, while an airway pressure below the critical closing pressure will cause the unit to approach closure in a similar fashion. In modeling the whole lung, Bates and Irvin combined many such units in parallel, assigning each airway distinct values for P_{crit}, S_o, and S_c from probability distribution functions. In choosing different values for parameters governing the distributions of the three parameters, the model demonstrated its ability to recreate a transient elastance increases due to airway derecruitment.

In contrast to its predecessor, our model examines a more general recruitment/derecruitment paradigm which allows separate critical opening and closing pressures (P_o and P_c) and velocities (S_o and S_c) for each airway (Figure 3). In this instance, the relationship governing the rate of change of an airway's location on the virtual trajectory is

$$\frac{dx(t)}{dt} = \begin{cases} s_o(P_{aw} - P_o) & P_{aw} > P_o \\ s_c(P_{aw} - P_c) & P_{aw} < P_c \\ 0 & otherwise \end{cases} \tag{9}$$

17

When opening and closing pressures are not equal, there is a potential region of stability, on which x is not changing and the airway does not tend toward transition. Once the airway pressure moves outside the region of stability the value of x will change as above.

Figure 3: Graphical representation of virtual trajectory used for R/D paradigm

Figure 4: Schematic of the distributed model of respiratory mechanics.
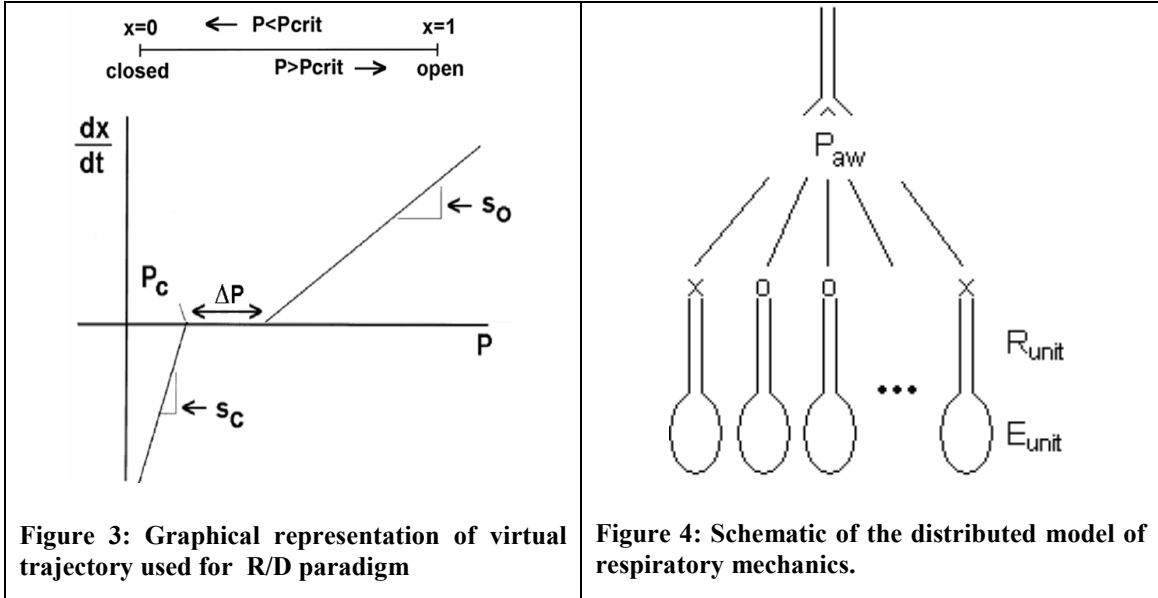
We also replaced the Salazar and Knowles pressure-volume model (54) used by Bates and Irvin (9) for each airway unit by a linear resistance in series with a linear elastic compartment that stores flow as a function of time (Figure 4). The relationship between pressure, volume and flow for each pathway is that of the linear single compartment model described above. Using this arrangement allows the lung to interact with a model of our mechanical ventilator, explicitly conserving flow by allowing each unit to dynamically accumulate volume. All lung units were given identical values for airway resistance, R_{unit}, and elastance, E_{unit}. We modeled the lung using 1,250 units arranged in parallel so each unit receives a common pressure, P_{aw}.

3.2   Origin of Experimental Data

The experimental data used for our model fitting come from previously made lung elastance measurements in healthy and lung injured mice (5). All experiments were performed in the Vermont Lung Center under direction of Gil Allen, M.D. A brief overview of the experimental protocol is provided to place the model and resulting data in an appropriate physiologic context. Experimental protocols were identical for healthy and injured mice except where indicated.

Under general anesthesia (400 mg/kg tribromo-ethyl alcohol via intraperitoneal injection) 8-10 week old female C57/BL6 mice were given deep oropharyengeal instillation of 75 μl of either sterile phosphate buffered saline at pH of 7.4 (controls) or pH 1.8 hydrochloric acid (injured). Mice were randomly assigned artificial ventilation and measurement of lung mechanics at 4, 14, 24 and 48 hours after instillation. Following induction of general anesthesia using intraperitoneal sodium pentobarbital (90 mg/kg), the mice were tracheostomised using an 18 gauge metal cannula. Each mouse was placed on the Flexivent (SIREC, Montreal, Canada) small animal ventilator. All mice were ventilated at target delivered volumes of 0.25 mL per breath at a rate of 180 breaths per minute. Ventilation was performed for 8.5 minutes at three levels of PEEP (1, 3, 6 cm H_2O) in random order. Two pressure limited deep inflations (rate of 30 per minute, P_{max} of 30 cmH_2O) were given preceeding each PEEP change to normalize volume history and recruit collapsed lung. Measurements of respiratory impedance were made every 15 seconds using the forced oscillation technique (5). Lung stiffness was measured by determining elastance, H, from fitting the constant phase model to the respiratory impedance spectra obtained using a two second broadband perturbation.

19

3.3 Modeling Whole Lung Behavior and Ventilator-Lung Interaction

In order to reliably simulate the conditions of the experiment, we modeled the interactions between our experimental ventilator and the lung (Figure 5). The ventilator breath is separated into two phases, with the inspiratory phase being driven by a volume-controlled linear piston, while the expiratory phase is passive due to elastic recoil of the respiratory system, against a static PEEP. Both of these phases have separate modeling equations that determine P_{aw} in the simulated lung.

The inspiratory phase of the breath is a quarter of a sinusoid, terminated at its peak. Each breath is delivered by moving a linear piston to displace a certain volume at a predetermined rate. The volume output from the ventilator, V_{cyl}, is divided between volume lost in gas compression, V_{gas}, and volume that proceeds into the breathing circuit. The compressed gas volume is given by

$$V_{gas}(t) = V_{gas}(t - \Delta t) + \Delta V_{cyl} - \Delta V_L \tag{10}$$

where ΔV_{cyl} is the change in cylinder volume and ΔV_L is the change in respiratory system volume between the previous data point, separated by a time step Δt. The pressure generated by compressing gas within the cylinder is given by

$$P_{gas}(t) = E_{gas} V_{gas}(t) \tag{11}$$

where E_{gas} is the elastic modulus of the gas. Because gas compression is a parallel process to the delivery of gas to the respiratory system, $P_{aw,}$ is equal to the pressure delivered to the respiratory system after accounting for the pressure drop that occurs through the ventilator tubing and tracheal cannula:

$$P_{aw}(t) = P_{gas}(t) - \frac{R_{eq}}{R_L(t-\Delta t)}\left[P_{aw}(t-\Delta t) - V_L(t-\Delta t)\cdot E_L(t-\Delta t)\right]$$

$$= P_{gas}(t) - R_{eq}\cdot \dot{V}_L(t-\Delta t) \tag{12}$$

Once the ventilator piston has reached its target displacement volume the expiratory phase is entered and respiratory function is supported only by a fixed PEEP. Pressure during the expiratory phase is determined by the lung's volume and elastic recoil.

$$P_{aw}(t) = PEEP + \sum_{N_{open}}\left[R_{unit}\dot{V}_i(t-\Delta t) + E_{unit}V_i(t-\Delta t)\right]$$

$$= PEEP + R_L\dot{V}_L(t-\Delta t) + E_L V_L(t-\Delta t) \tag{13}$$
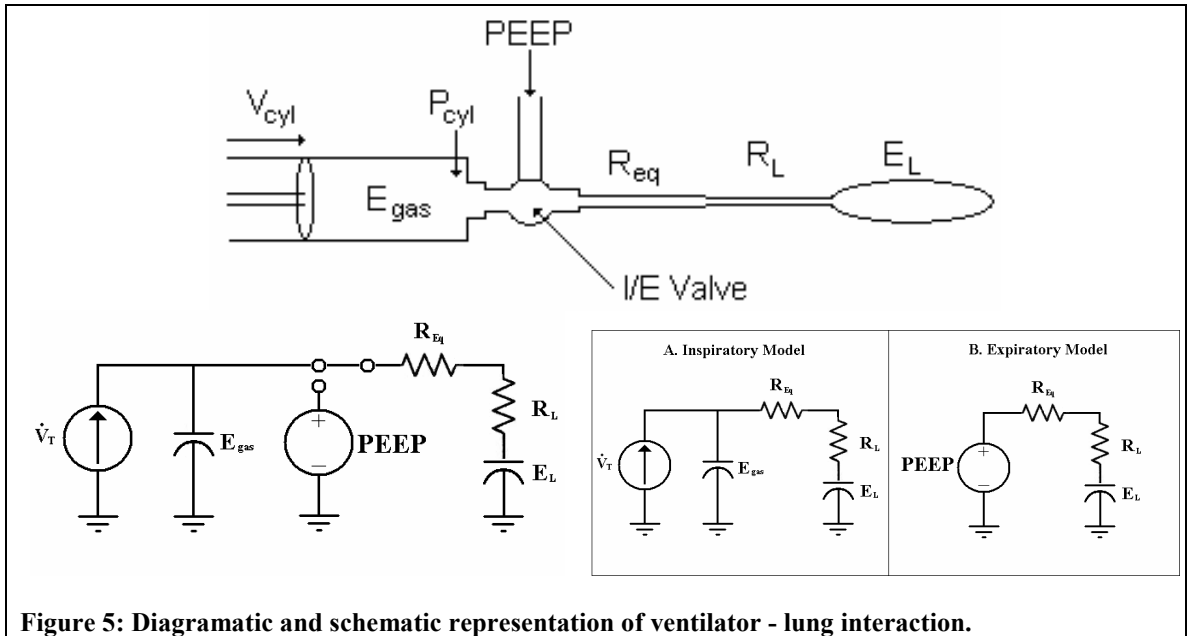
Figure 5: Diagramatic and schematic representation of ventilator - lung interaction.

Airway pressure is used to calculate the state of recruitment by changing the value of x as described above and opening or closing new lung units as appropriate. Global lung mechanics are, in turn, calculated as function of the newly determined state of recruitment in the sense that the resistance and elastance of the whole lung depend on the number of airways participating in ventilation. Noting that closed airways will have zero

conductance and zero compliance we obtain expressions for R_L and E_L as a function of recruitment:

$$R_L(t) = \left(\sum_{i=1}^{N} \frac{1}{R_i} \right)^{-1} = \frac{R_{unit}}{N_{open}(t)} \qquad E_L(t) = \left(\sum_{i=1}^{N} \frac{1}{E_i} \right)^{-1} = \frac{E_{unit}}{N_{open}(t)}. \qquad (14)$$

These relationships demonstrate that, in general, the properties of the lung's resistance and elastance are governed by time varying parameters that hyperbolically decrease as a function of open lung.

Flow for each open airway at time t is determined by rearranging the equation of motion for the single compartment model.

$$\dot{V}_i(t) = \frac{1}{R_{unit}} \left(P_{aw}(t) - V_i(t - \Delta t) E_{unit} \right) \qquad (15)$$

Total flow into the respiratory system can then be determined by summation of individual airway flows over all i

$$\dot{V}_L(t) = \sum_{i=1}^{N} \dot{V}_i(t) = \sum_{i=1}^{N} \frac{1}{R_{unit}} \left(P_{aw}(t) - V_i(t - \Delta t) E_{unit} \right) \qquad (16)$$

Similarly, the volumes in each airway and in the whole lung can be found by summation in time, which in our discrete case simply consists of adding the present volume increment to the volume at the previous time point:

$$V_L(t) = V_L(t - \Delta t) + \dot{V}_L(t)\Delta t \quad ; \quad V_i(t) = V_i(t - \Delta t) + \dot{V}_i(t)\Delta t \qquad (17)$$

We have verified analytically that computing total flow into the lung based on global lung mechanics gives the same flow as individually summing flows over all the open elements:

$$\dot{V}_L(t) = \frac{P_{aw}(t)}{R_L} - \frac{E_L}{R_L} V_L(t - \Delta t)$$

$$\sum_{i=1}^{N} \dot{V}_i(t) = \sum_{i=1}^{N} \frac{1}{R_{unit}} \left(P_{aw}(t) - V_i(t - \Delta t) E_{unit} \right) \tag{18a}$$

$$= \sum_{i=1}^{N} \frac{P_{aw}(t)}{R_{unit}} - \sum_{i=1}^{N} \frac{V_i(t - \Delta t) E_{unit}}{R_{unit}}$$

Because the relationship only applies to airways participating in ventilation

$$= N_{open} \frac{P_{aw}(t)}{R_{unit}} - \frac{E_{unit}}{R_{unit}} \sum_{i=1}^{N} V_i(t - \Delta t)$$

$$= N_{open} \frac{P_{aw}(t)}{R_{unit}} - \frac{N_{open}}{N_{open}} \frac{E_{unit}}{R_{unit}} V_L(t - \Delta t) \tag{18b}$$

$$= \frac{P_{aw}(t)}{R_L} - \frac{E_L}{R_L} V_L(t - \Delta t)$$

In order to ensure that ventilation is appropriately distributed we compute flows individually to each airway, since the flow they receive is inversely related the present volume of the unit.

Initial validation of the model system was performed by analyzing its behavior over the course of several ventilator breaths. This analysis was performed with all airways initially closed using distributions of recruitment/derecruitment parameters that favor a stable, mostly-open lung. Original choices of time step, Δt, were insufficient in characterizing the pressure, volume and flow consistently over adjacent breaths. Low sampling rates were noted to cause breath initiation before the previous exhalation fully terminated, resulting in "virtual air trapping" at higher lung volumes and longer respiratory time constants. In this phenomena, there is not enough temporal resolution to capture complete exhalation at end expiration. Initialization of the subsequent breath begins at higher lung volume, and lung volume increases without bound. Early

23

simulations demonstrated that the model also required an even number of time points per breath, synchronized to identical points within each cycle in order to prevent adjacent breaths from varying in 2-4 breath couplets. At a ventilator rate of 180 breaths per minute a sample rate of 60 Hz was found ideal in removing variability between breaths while imparting only modest computational burden (~100,000 time steps per simulation). Once the appropriate time step was determined the model's opening behavior was examined from a closed state at varying tidal volumes and values of R_{unit} and E_{unit}. Peak airway pressure and the extent of recruitment were found highly dependant on the values of V_T and E_{unit}. Final values for R_{unit} and E_{unit} were chosen as 2,500 cmH$_2$O s L^{-1} and 27,500 cmH$_2$O L^{-1} to ensure that the near fully recruited lung is mechanically similar to the healthy lung; the value of V_T was chosen to match experimental conditions.

3.4   Simulations

Our initial simulations test the impact of model architectures on the goodness of fit by comparing various adaptations of the model to the average elastance time courses from each experimental condition (control and injured at 4 times post-instillation). Following objective model comparison (detailed below) the best fit model was used for parameter estimation using each of the experimental elastance profiles from the individual mice.

In all simulations we have assumed that the opening and closing velocities for each airway, So and Sc, are described by hyperbolic distributions, each characterized by one free parameter, s_o or s_c, so that

$$So \sim \frac{s_o}{unif[0,1]} \quad ; \quad Sc \sim \frac{s_c}{unif[0,1]}. \tag{19}$$

24

The closing pressure distribution was modeled as Gaussian with parameters Pc_μ and Pc_σ governing the mean and standard deviation respectively. We have posed four potential models to fit the experimental data (Figure 6). In the simplest model, opening pressures and opening velocities were set equal to the closing pressures and velocities. We have separately examined the effects of allowing the opening and closing velocities to be unequal, as well as shifting the mean of the opening pressure distribution a constant amount, ΔP, relative to the closing pressure distribution. Finally, simulations were performed where both changes were incorporated into to the model.

Each simulation begins with an initialization routine consisting of 30 seconds of ventilation at a PEEP of 1 cmH$_2$O, providing a standard baseline from which all recruitment maneuvers are
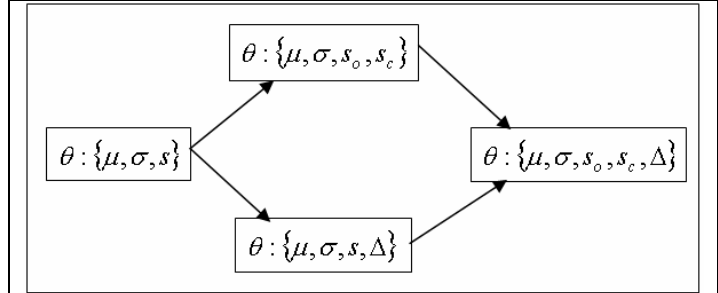
Figure 6: Model evolution from 3 to 5 parameters, with 2 intermediate varients.
Separation of slopes and pressures are done in parallel, then combined.

performed, mimicking the conditions in the experimental protocol. After initialization, a two-breath deep inflation is performed to recruit collapsed lung and ventilation proceeds for 8.5 minutes. The ventilation sequence is repeated from the baseline state for ventilation over PEEP levels of 1, 3 and 6 cmH$_2$O. The model simulates ventilation by repeatedly calling a subroutine to simulate 15 seconds of ventilation, ending with an estimate of the respiratory system elastance, E. Each call to the subroutine uses the ending respiratory state from the previous function call as the initial values for the next 15 seconds of ventilation. All measurements are synchronized to the experimental

measurements and were obtained by curve fitting the single compartment equation of motion

$$P_{aw}(t) = R\dot{V}_L(t) + EV_L(t) \tag{20}$$

to pulmonary pressure, volume and flow over the course of 4 breaths. Once the entire elastance time course has been simulated, the values at each point are compared to the experimental values and the error quantified.

All simulations were run on a Dell Pentium 4 desktop computer with CPU clock speed of 3.40 GHz and 1.00 GB of ram. Simulations were written and performed using the Matlab software package (Mathworks, Natick MA) running under Microsoft Windows XP. Each iteration of the model takes 28 seconds to initialize the model and produce the elastance values from the ventilation course at all three levels of PEEP.

3.5 Model Fitting

Parameter estimation was performed by minimization of Φ_M, the root mean square error between model elastance, E_M, and experimental elastance, $H(t_i)$,

$$\Phi_M = \sqrt{\frac{1}{K}\sum_{i=1}^{K}(E_M(\theta,t_i) - H(t_i))^2} \tag{21}$$

where K is the number of elastance measurements and θ is the vector containing current values of parameters being estimated. Initial attempts at fitting the model were made using a grid search algorithm. Due to the tortuous nature of the parameter space the best fit solution was highly dependent on the initial grid points chosen and local, rather than global minima were often reached. This strategy also required an excessive number of iterations to result in convergence, especially given the fine nature required of the starting

26

grid in order to increase the probability of capturing the global minimum. For a grid with equal numbers of points per parameter the computational time, T, increases exponentially as a function of grid size, S, in points per parameter, and as a power function of the length of the parameter vector, L:

$$T = T_o S^L \tag{22}$$

where T_o is the duration of one iteration. Computational time for this approach is shown in Figure 7 for various grid sizes and parameter numbers with T_o at 28 seconds.

	5	6	7	8
5 Parameters	24.30555556	60.48	130.7211111	254.8622222
4 Parameters	4.861111111	10.08	18.67444444	31.85777778
3 Parameters	0.972222222	1.68	2.667777778	3.982222222
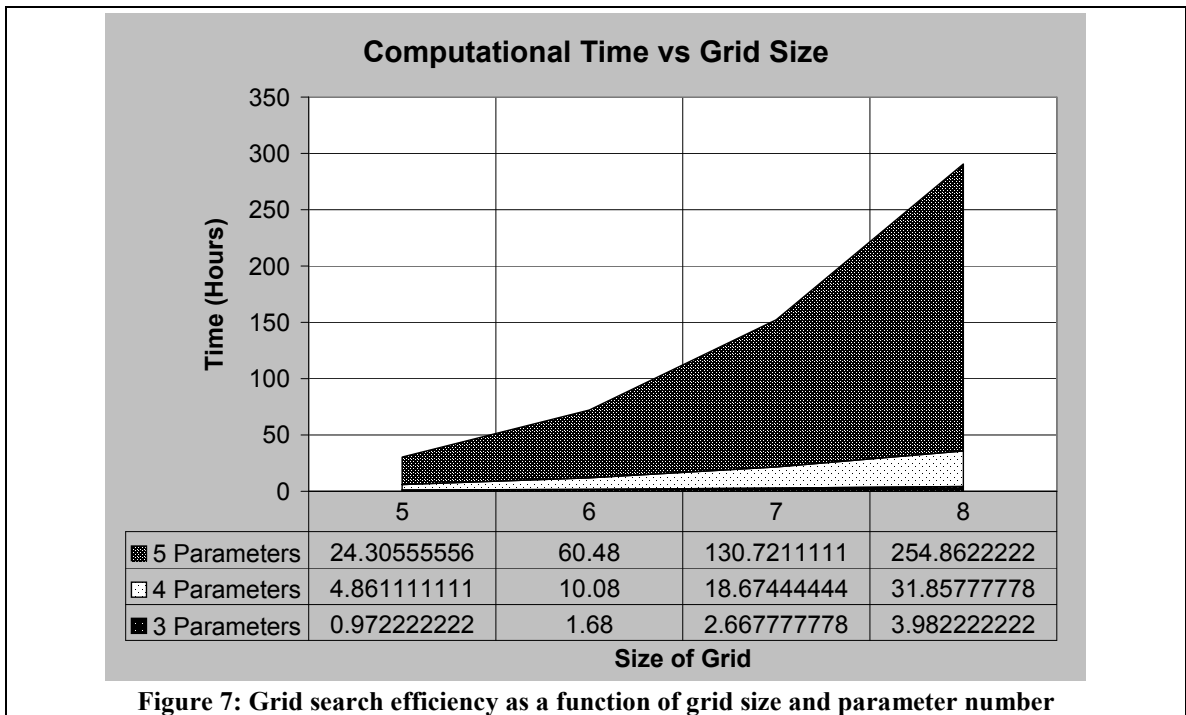
Size of Grid

Figure 7: Grid search efficiency as a function of grid size and parameter number

An adaptive grid search strategy was investigated, however the fit's sensitivity to the location of initial grid points was found to predominate over grid size or number of adaptations. Logarithmically spaced grids were also investigated without any significant reduction in computational burden and no increase in reliability or accuracy. This fitting approach was abandoned early in the course of the project, as its unreliability necessitated

frequent observation of simulation progress and the repeated rerunning of simulations at substantial computational times.

In considering the number of parameters, the duration of each iteration and lack of closed form solution to the fitting problem, we next examined the Nelder and Mead simplex minimization algorithm (46) to estimate the values of the parameters that best characterize the data. This method uses a geometric approach to traversing an L dimensional error space. This approach to model fitting can be most simply understood by examining a visual example in a two-dimensional parameter space (Figure 8). The model begins by evaluating the model at a user specified initial condition $\theta_0 = \{X_{1_0}, X_{2_0}\}$ and storing the error value $\Phi(\theta_0 = \{X_{1_0}, X_{2_0}\})$.

A geometric "simplex" is generated by evaluating the model at one additional point for each parameter in the model. For this example case, two additional points are required, creating a triangle in the two-dimensional space. Our implementation of this method chooses the additional

Figure 8: Diagrammatic representation of traversal of a 2-D parameter space using a simplex optimization method
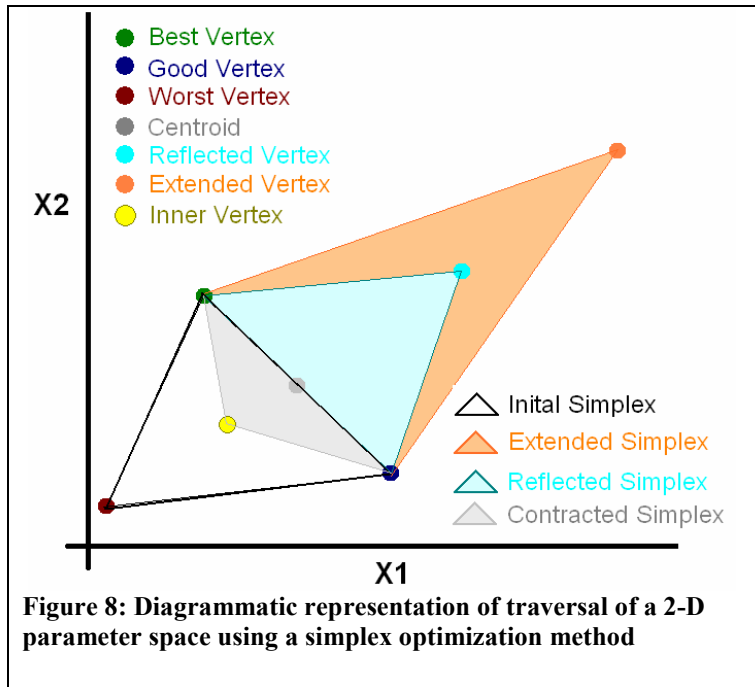
points by adding 10% to one parameter at a time so that the three vertices of the initial simplex are the triangle composed of points:

28

$\left\{ \left[X_{1_0}, X_{2_0} \right] \left[1.10 \times X_{1_0}, X_{2_0} \right] \left[X_{1_0}, 1.10 \times X_{2_0} \right] \right\}$. We desire to move this simplex until we are within a certain resolution of either the minimum value of the function or until the parameter changes are appropriately minute. To do this we begin by labeling each of the vertices based on their residual error so the comparatively best (point B), intermediate (point I) or worst (point W) vertices are represented by the green, blue and red vertices in Figure 8 respectively. We also label the midpoint of the axis created by the line segment $\overline{BI}$ through the two best points as the "centroid" (point C) of the simplex. A reflection of point W about $\overline{BI}$ produces the vertex R (light blue in Figure 8), where the function is evaluated. A set of rules is used to determine the location of the next point based on comparison of the residual errors at each point:

1. If $\Phi(\theta = B) < \Phi(\theta = R) < \Phi(\theta = W)$: Replace W with R and reevaluate $\Delta(BIR)$, the light blue triangle in Figure 8. (Reflection of the simplex)

2. If $\Phi(\theta = R) < \Phi(\theta = B)$: Extend the simplex by evaluating the point E by doubling the value of R so E lies at twice the distance from the centroid, along the line $\overline{WCR}$

   a. If $\Phi(\theta = E) < \Phi(\theta = R)$: Replace W with E and evaluate $\Delta(BIE)$, the orange triangle in Figure 8. (Extension of the simplex)

   b. If $\Phi(\theta = E) < \Phi(\theta = R)$: Replace W with R and evaluate $\Delta(BIR)$, the light blue triangle in Figure 8. (Reflection of the simplex)

3. If $\Phi(\theta = W) < \Phi(\theta = R)$: Contract simplex and replace W with the midpoint of $\overline{WC}$, inner vertex I, generating the grey triangle in Figure 8. (Contraction of the simplex)

29

Combinations of the reflection, extension and contraction operations above are generally sufficient to traverse a fairly well behaved parameter space. In general, this approach is robust enough to identify parameters whose values may span over 7 orders of magnitude (8). Sensitivity to initial conditions was considerably diminished and minima reliably determined from reasonable initial guesses based on crude estimates from a rough grid search. Termination criteria for the optimization method were chosen so that relative function changes fell within 5×10^{-4}, while relative tolerances on the parameters were below 5×10^{-4} percent. This was generally achieved in under 250 iterations, costing roughly 2 hours of computational time per fit.

Our initial simulations test the impact of model architectures on the goodness of fit by comparing adaptations of the model to the average elastance time courses from each experimental condition (healthy and injured at 4 time points). Following objective model comparison (detailed below) the best model was fit to each of the elastance profiles from the individual mice for parameter estimation from each subject.

3.6 Model Comparison

All models were fit to the average elastance time courses within each of the 8 study groups (control and injured mice at each of the 4 time points) for the purpose of identifying models capable of capturing the trends in dynamic collapse. In order to objectively compare the models, we have employed the corrected Akaike Information Criterion (AIC_C) (2, 13)

$$AIC_C = K \ln\left(\frac{SSR}{K}\right) + 2(L_\theta + 1) + \frac{2(L_\theta + 1)(L_\theta + 2)}{K - L_\theta} \qquad (23)$$

where L_θ is the length of the parameter vector for a given model and SSR is the sum of squared residuals between a given model fit and the data. Since our performance criteria for minimization was a root mean square error, our AIC_C score was computed as

$$AIC_{C,M} = 2K\ln(\Phi_M) + 2(L_\theta + 1) + \frac{2(L_\theta + 1)(L_\theta + 2)}{K - L_\theta}. \tag{24}$$

This measure was chosen since it allows simultaneous comparison of several models with different degrees of freedom at substantial penalty for the addition of free parameters, choosing the model that best characterizes the data in the maximum likelihood sense. The AIC_C was computed for each model on for each experimental condition and comparisons were made across all models for each condition. Using the differences between AIC_C scores for a given model and the model with minimum AIC_C

$$\Delta(AIC_{C,M}) = AIC_{C,M} - \min\{AIC_{C,j}\}, \tag{25}$$

probabilities that a particular model, M, best describes the data were determined as

$$P(\Phi_M|D) = \frac{\exp\{-\tfrac{1}{2}\Delta(AIC_{C,M})\}}{\sum\limits_{j=1}^{4}\exp\{-\tfrac{1}{2}\Delta(AIC_{C,j})\}}. \tag{26}$$

The model with the highest Akaike derived probability can thus be considered the candidate model with the maximum likelihood from those models tested.

3.7 Parameter Estimation, Comparison of Groups

Once the best fit model was chosen, parameter values for each mouse were determined by fitting the model to the individual subjects. Within each of the 8 groups of subjects the means and standard deviations were obtained on each parameter. Comparison of statistical significance between groups was performed using a two-way

31

Analysis of Variance (ANOVA) to assess the independent effects of injury and time after instillation, as well as the combined effect of injury over time. All two-way ANOVA calculations were performed using the statistics toolbox in Matlab.

In order to show the differences in parameter distributions we have reconstructed probability distribution functions for the critical pressures and velocities based on the average parameter values from each condition. Plots of the rate constant distributions display histograms of the actual distribution of *So* and *Sc* from each simulation. Using a one parameter hyperbolic distribution virtually assures a few dramatic outliers that possessed extraordinarily fast opening or closing rates. To handle presenting this visually, all histograms were truncated to lump airways with rate constants outside of the range [.0025, 2] into the right-most bin. Inclusion of the exact values of these few, sparse airways would dramatically influence the appearance of the histograms and obscure the distribution of the vast majority of the airways participating in ventilation. Visualization of the critical pressures was done by plotting Gaussian distributions using estimated means and standard deviations. All healthy subjects were pooled together, as no significant changes in parameters was observed in these groups.

3.8   Sensitivity Analysis

For the model determined most likely in explaining the data given the Akaike scores, sensitivity analysis was performed about each minimum to see how well each mouse's elastance fit is described by an individual parameter. For each individual mouse the sensitivity to each parameter, S_i, was assessed by determining the fractional change in model error for a given perturbation to each parameter value

$$S_i = \frac{\partial \Phi}{\partial \theta_i} = \frac{\left(\dfrac{\Phi_P - \Phi_0}{\Phi_0}\right)}{\left(\dfrac{\theta_P - \theta_0}{\theta_0}\right)}$$

where θ_0 and Φ_0 are the optimal parameter values and corresponding error, while θ_P and E_P represent the parameter value and error associated with the perturbation from the optimal value. Fractional change in error was chosen so that the error change could be compared between subjects and across groups.

To compare model sensitivities to Pc_σ, Δ, S_O, and S_C each of these parameters was changed by a 5% perturbation about the optimum value in both the positive and negative directions. The perturbation chosen for Pc_μ was the addition or subtraction of 0.25 cmH_2O to the parameter value. This was chosen because fractional changes to the control values were nearly negligible, due to their proximity to zero. Additionally, since some values of Pc_μ were below zero, fractional changes in the values would not allow for zero crossing. Finally, physiologic changes in this parameter between health and disease appear additive rather than multiplicative. Normalization of the change in error by the relative change in each parameter value allows the comparison of sensitivity directly between parameters. Where applicable, isosurfaces of the error space for pairs of parameters were investigated to determine how error covaries in the region of a solution.

Chapter 4   Results

4.1   Verification of Model Behavior

In order to validate the model's ability to faithfully recreate ventilator-lung interactions we first examined its response to the ventilator waveform used experimentally over several breaths. Figure 9 shows the airway pressure, lung volume and flow upon being ventilated from the fully closed state. The high pressure generated in the first few breaths begins to recruit new flow pathways, decreasing the lung's apparent resistance and elastance. As the lung opens, peak airway pressures fall, while the total lung volume and total pulmonary flow increase.

Figure 9: Model response to ventilation from a fully closed state.
A. Airway pressure. B. Lung Volume. C. Pulmonary Airflow. D. Fraction of lung that is open. Note that as the fraction of lung increases airway pressure decreases, while flow and volume increase until the fraction of open lung reaches an approximate steady state.
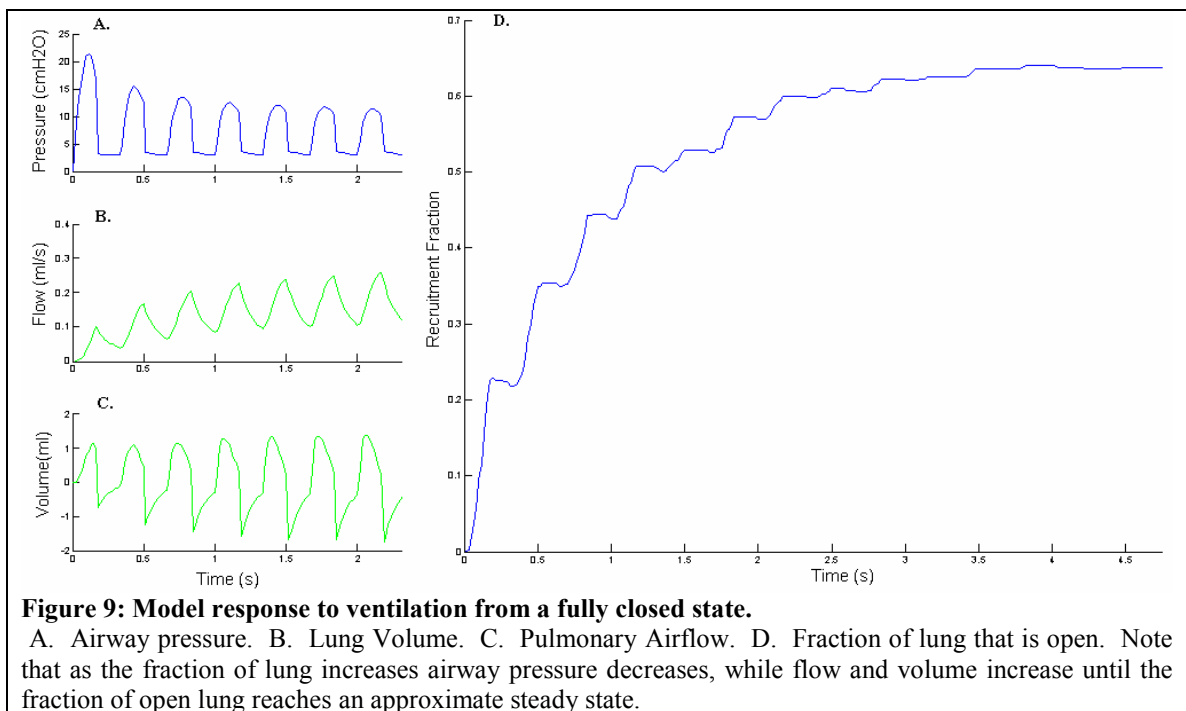
Recording the flow and volume from a sample of airways during the initial and final breaths of the initialization routine demonstrates that regional heterogeneity of ventilation decreases as the state of recruitment stabilizes (Figure 10). It should be noted that intratidal derecruitment occurs profoundly during the initial onset of ventilation

34

(Figure 9. D, Figure 10). Recruitment reduces the peak to peak variability in flow and volume, as well as the occurrence of intratidal collapse and reopening (Figure 10). During the initial breaths, few lung units are open and most of the tidal volume is captured by relatively few airways resulting in high airway pressures, high regional flows and overdistension. The maximum flows for the initial breaths are four times higher than in the steady state condition, while the peak volumes are twice as high.

Figure 10: Sample flow and volume profiles
Comparison of flow (top) and volume (bottom) from a sample of 40 airways during the initial (left) and final (right) two breaths of the initialization routine.
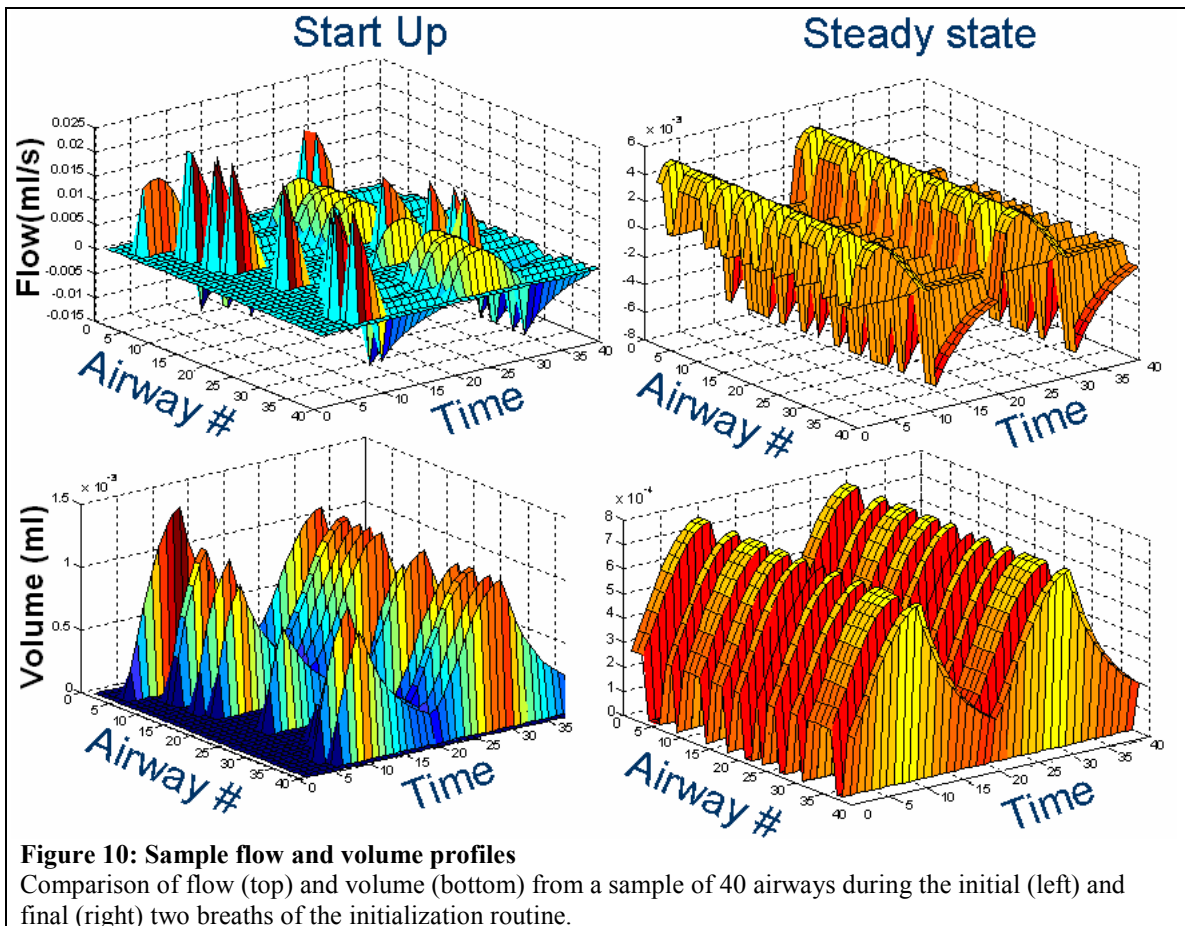
4.2   Model Fits to Average Elastance Time courses

We have begun by fitting each of the 4 proposed models to the healthy elastance data, beginning with the simplest model (3 parameters). Figure 11 shows the average

elastance time courses for healthy mice at each of the 4 time points, as well as the best fit

at each time point for each proposed model. In each figure, experimental data are

Figure 11: Experimental data from healthy mice shown with each model fit
A: 3 Parameter. B: 4 Parameter – critical pressures the same, opening and closing velocities separated.
C: 4 Parameter – velocities the same, opening and closing pressures separated. D: 5 Parameter –
opening and closing velocities and pressures different.
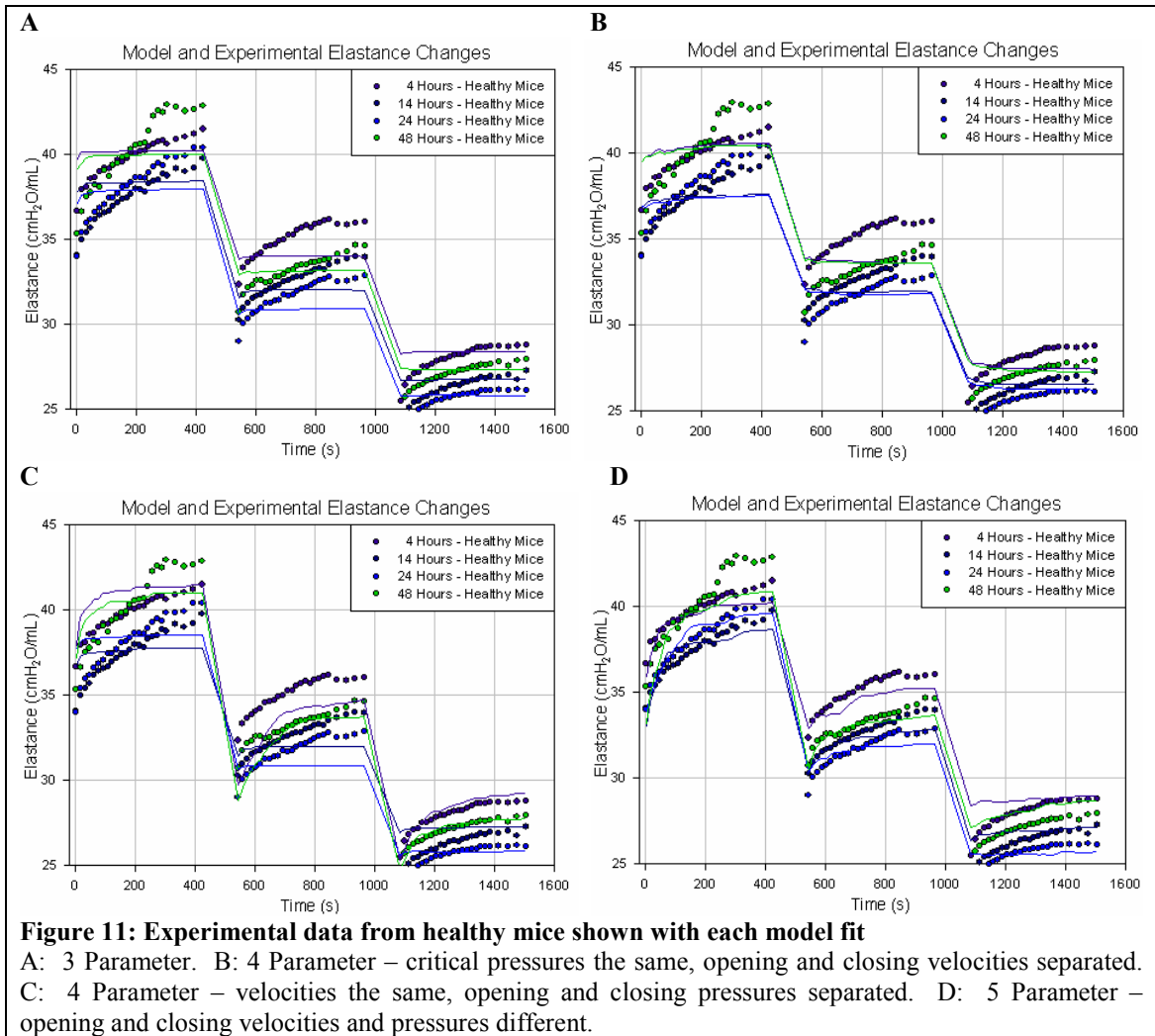
given by the closed circles, while model elastances are given by the solid lines. The three

parameter model (Figure 11 .A) was barely able to recreate any PEEP responsiveness and

possessed no significant dynamic behavior following deep inflation. Additionally, this

model was unable to demonstrate full recruitment of collapsed lung in response to deep

inflation. Introducing a constant separation of opening and closing velocities produced

very little qualitative or quantitative differences in model fits (Figure 11 .B). Allowing

36

the opening and closing pressures to be unequal produced a dramatic improvement in the model's ability to recreate some dynamics of collapse, as well as improving the initial recruitment response following deep inflation (Figure 11.C). In allowing both opening and closing velocities and pressures to differ, the model had far greater ability to recreate the initial response to recruitment maneuvers, PEEP response and dynamics of collapse seen experimentally (Figure 11.D and 8). Model residual errors are quantified and displayed with those from the injured data in Table 1 and Figure 14 below.

Figure 12: Experimental data from injured mice shown with each model fit
A: 3 Parameter. B: 4 Parameter – critical pressures the same, opening and closing velocities separated. C: 4 Parameter – velocities the same, opening and closing pressures separated. D: 5 Parameter – opening and closing velocities and pressures different.
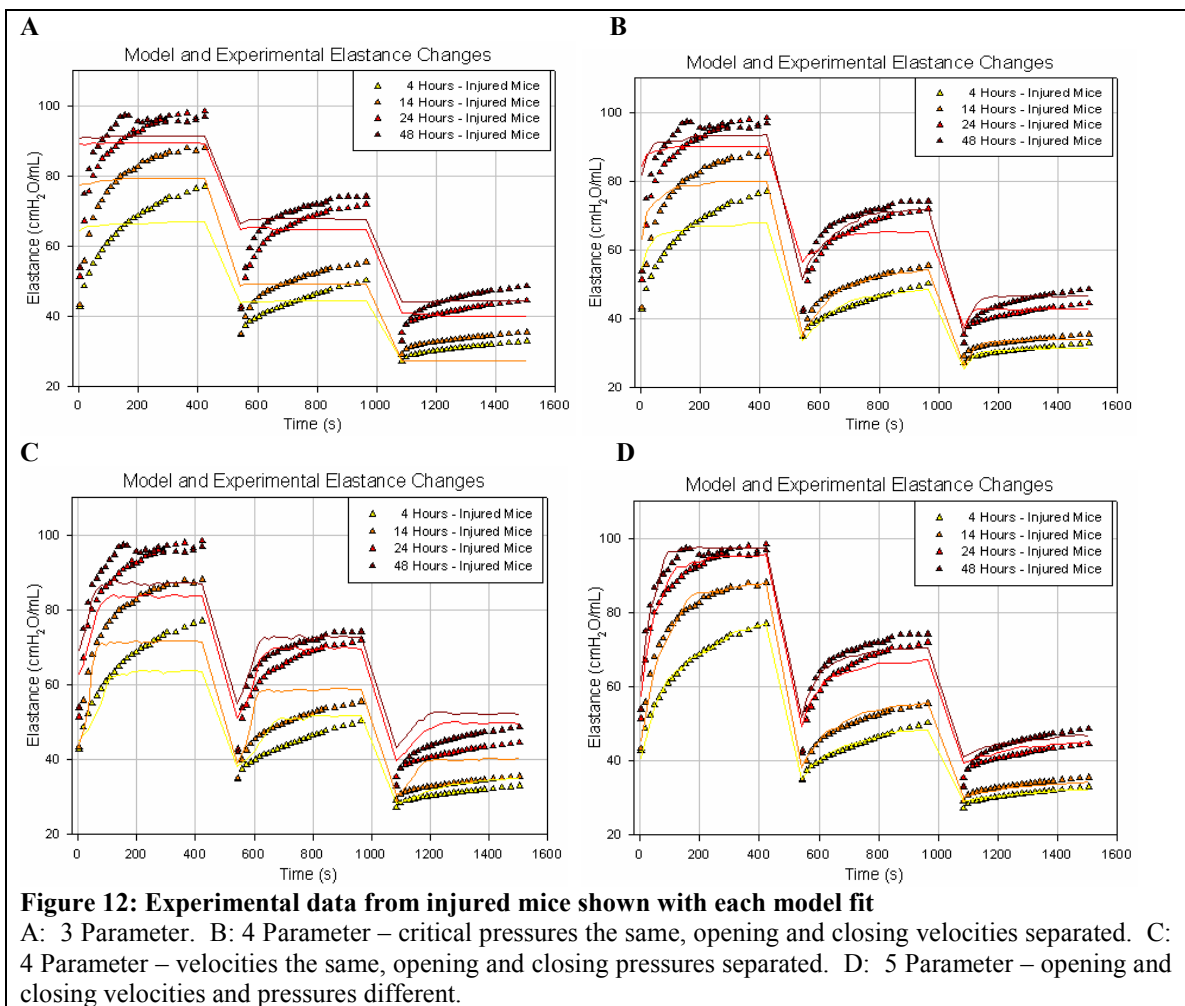
Model elastances obtained by fitting the model to the average injured data at each time point following instillation are shown in Figure 12 with solid triangles representing

stiffness from the experimental data and solid lines representing the model fits. Similarly

to what is seen in the healthy mice, the three parameter model is incapable of recreating

any significant dynamic recruitment/derecruitment behavior (Figure 12.A). Allowing the

opening and closing velocities to differ introduces some dynamic response and ability to

recreate PEEP dependence (Figure 12.B). This model is not recruitable enough following

deep inflation and the dynamics of collapse are not correct, in particular at low PEEP and

as the duration following injury increases.   Separation of the opening and closing

pressures considerably improves the recruitment response after DI and matches the early

time course of elastance changes, however this model plateaus quickly and does not

allow for more gradual collapse (Figure 12.C). The five parameter model is able to

successfully recreate the dynamics of the recruitment response and subsequent collapse at

all three levels of PEEP (Figure 12.D and Figure 13).

Figure 13: Best model ealastance values when fit to the average experimental data
Circles and Triangles represent the experimental data from healthy and injured mice respectively, while solid lines are the model elastances using the 5 parameter model.
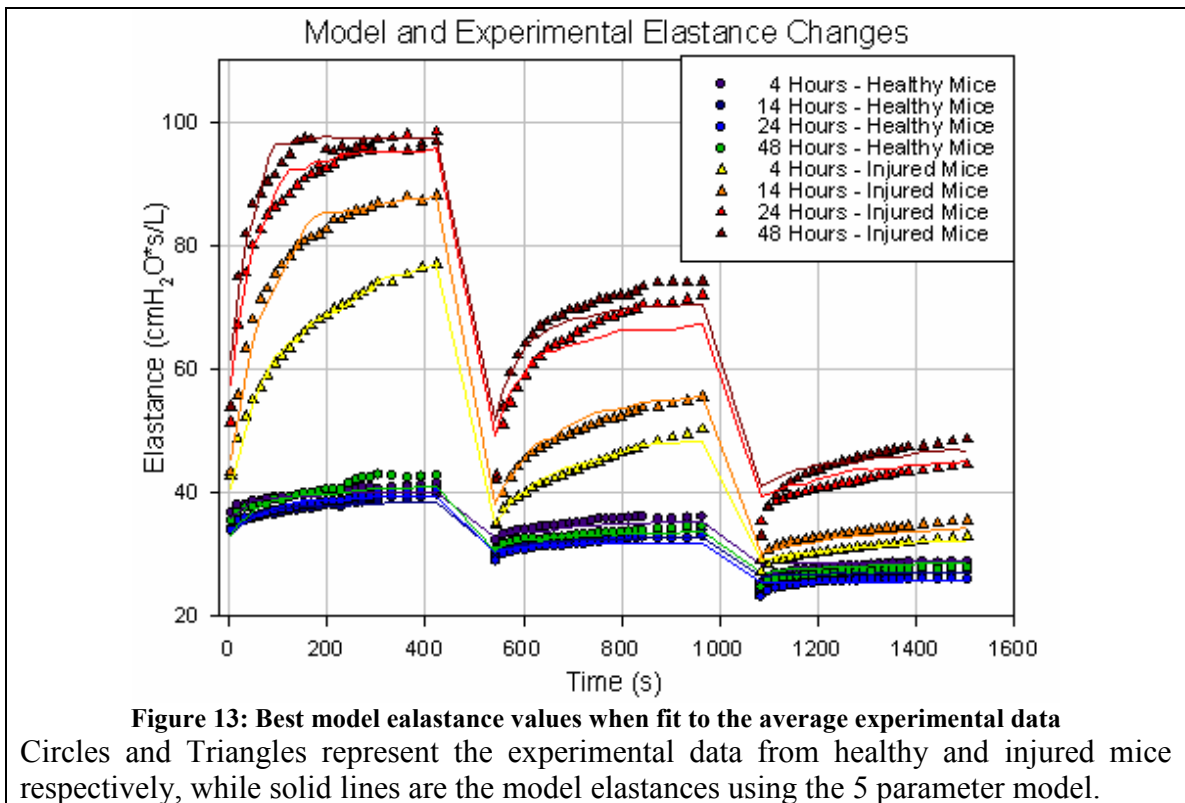
4.3 Model Comparison and selection

The residual errors for each model and each average time course are summarized in Table 1 and Figure 14. In all experimental conditions the residual error is lowest for the 5 parameter model. Probabilities that each model characterize the data were made from Akaike scores in order to choose the best model (in the maximum likelihood sense) while appropriately penalizing the addition of free parameters. Table 2 demonstrates that these probabilities strongly favor the 5 parameter model with separate opening and closing rate constants and pressures, despite the additional degrees of freedom.

The best model fits (solid lines) are shown with the experimental data (colored triangles) enlarged in Figure 13. The average root mean square error on all fits is 1.003.

Figure 14: Comparison of errors as function of model architecture, time and injury condition
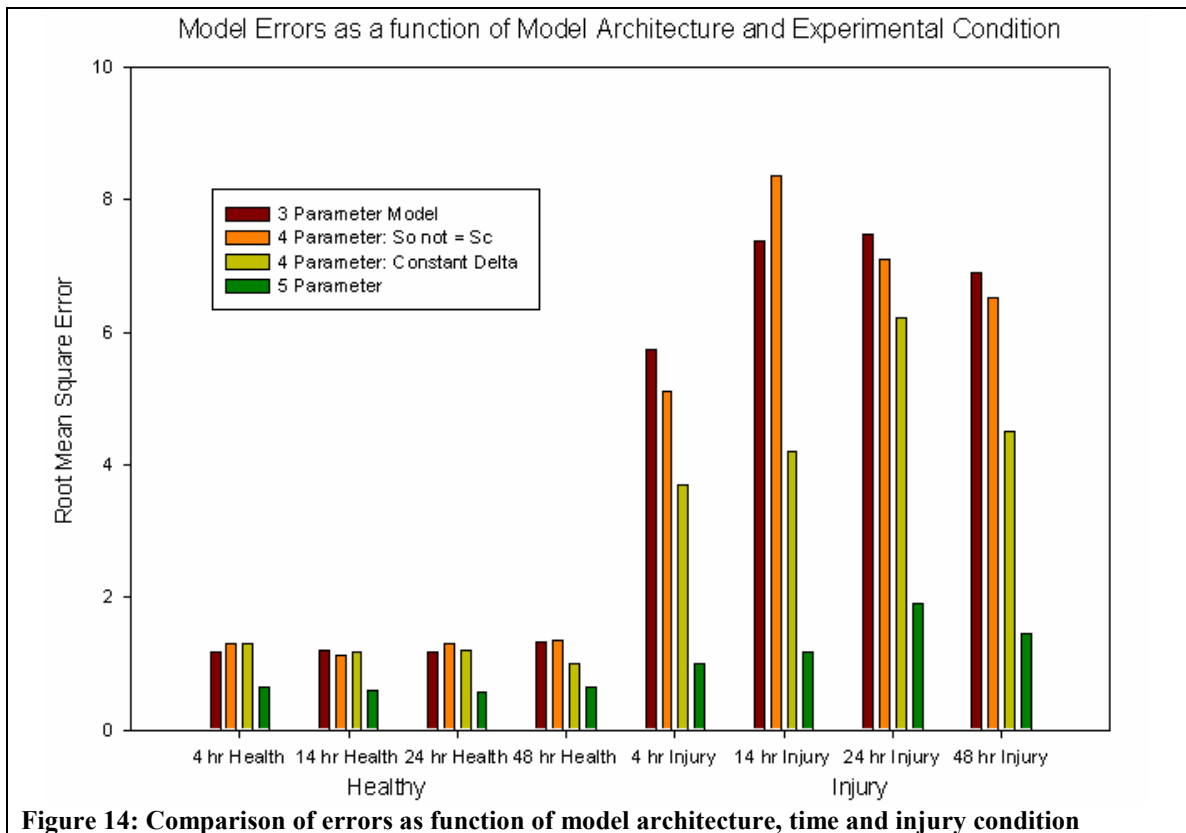
Table 1: Root mean square errors for each model and condition					
	Model	A	B	C	D
Healthy	4 Hour	1.1832	1.3104	1.2921	0.64481
	14 Hour	1.209	1.1225	1.1745	0.59231
	24 Hour	1.1828	1.3058	1.1956	0.58458
	48 Hour	1.3369	1.362	1.0064	0.65923
Injured	4 Hour	5.7275	5.1132	3.7023	0.9959
	14 Hour	7.3834	8.3474	4.2084	1.1816
	24 Hour	7.4686	7.0867	6.2062	1.9201
	48 Hour	6.8924	6.5281	4.4925	1.4492

Table 2: Akaike probabilities for each model and condition					
	Model	A	B	C	D
Healthy	4 Hour	2.64E-08	3.02E-10	4.78E-10	1
	14 Hour	8.23E-10	2.94E-09	6.72E-10	1
	24 Hour	1.09E-09	1.39E-11	2.45E-10	1
	48 Hour	1.02E-09	1.76E-10	3.36E-06	0.999997
Injured	4 Hour	1.83E-24	2.34E-23	8.65E-19	1
	14 Hour	1.22E-25	7.16E-28	3.49E-18	1
	24 Hour	6.22E-19	1.09E-18	8.24E-17	1
	48 Hour	8.9E-22	1.66E-21	3.21E-16	1

4.4 Model Fits on Individual Experimental Data

By averaging the elastance time courses over each condition we obtained a mean fit profile that was compared to the mean and standard deviation of the experimental data. Shown below in Figure 15 are the average model fits to the experimental data from all 4 healthy conditions, while the average injured fits are shown in Figure 16. In both cases only several data points from the mean curve fell outside the standard error of the

experimental measurements Table 3. It should be noted that the model fits have a variance that can not be directly separated from the experimental variability, so no standard deviation of the fit is displayed on these graphs. Average root mean square errors for each condition are summarized in Table 4 below. Note that these are the averages of the fitting errors in each condition, rather than the error between the average fit and the average data.

Figure 15: Mean model fit compared with average experimental data - Healthy Mice
Data shown as mean +/- standard deviation for healthy mice, with at 4, 14, 24, 48 hours.

Figure 16: Mean model fit compared with average experimental data – Injured mice
Data shown as mean + standard deviation for injured mice at 4, 14, 24, 48 hours.
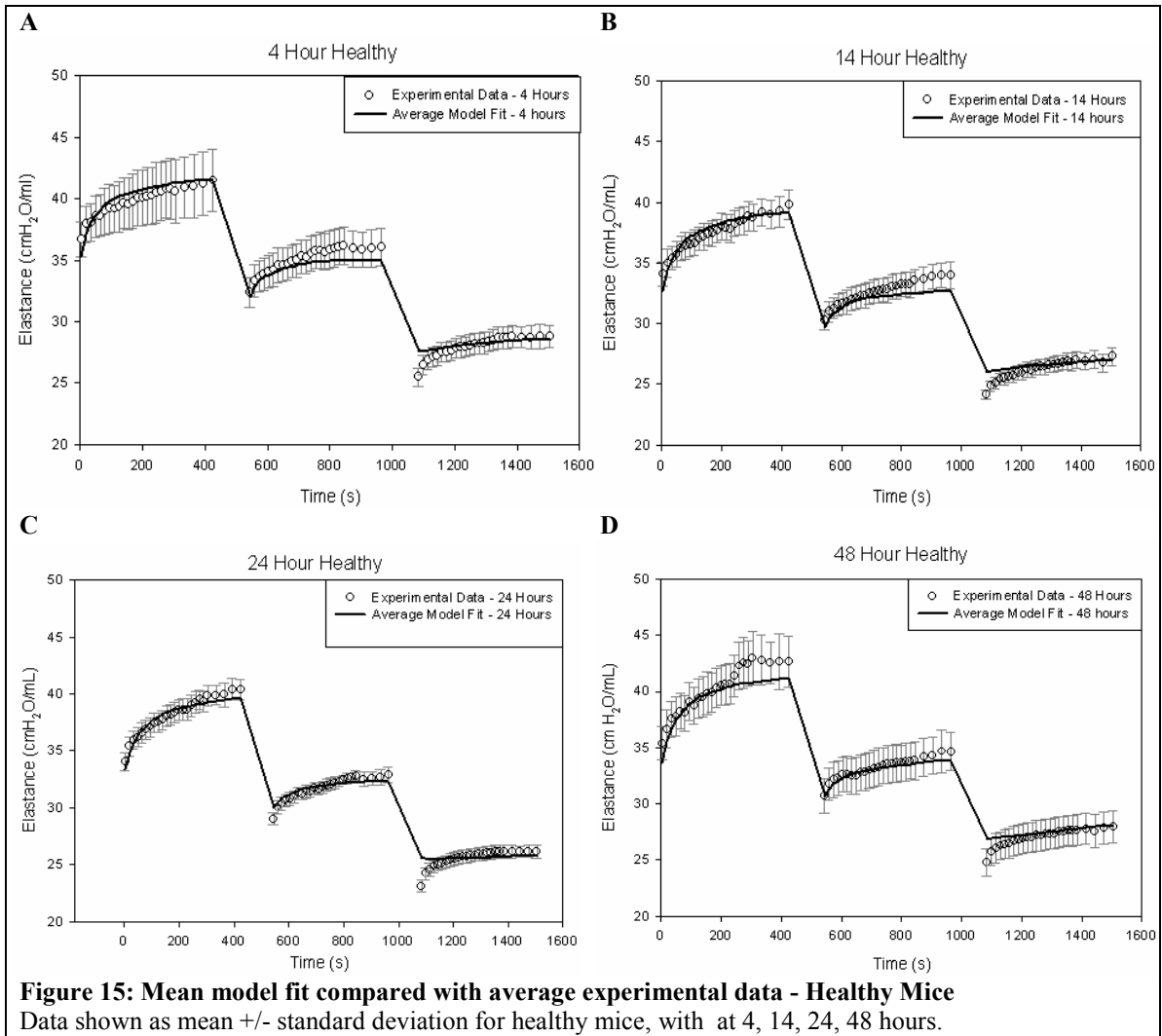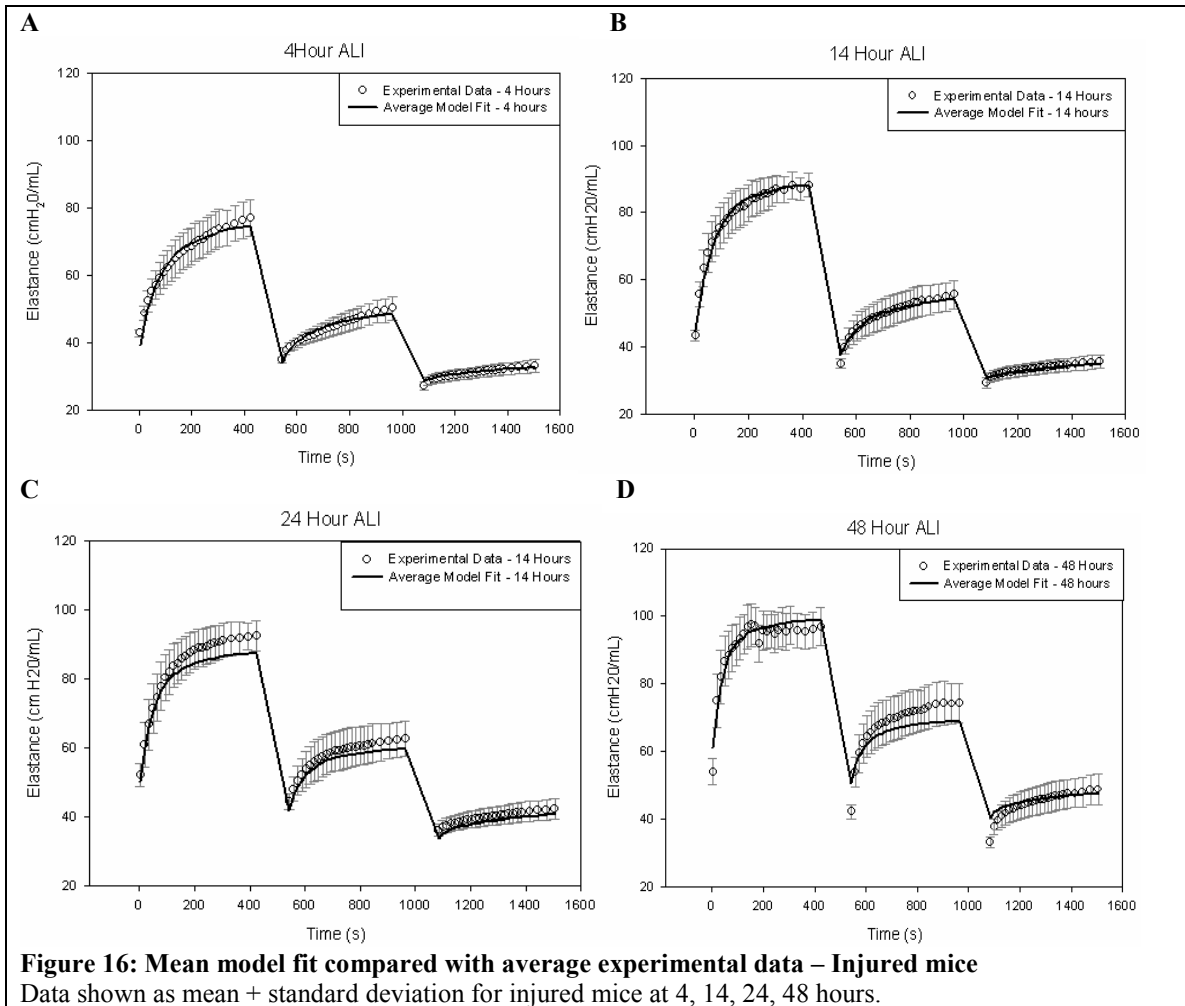
Table 3: Percentage of model points falling outside mean +/- standard error of data				
	4 Hour	14 Hour	24 Hour	48 Hour
Health	5.333333	10.66667	5.333333	2.666667
Injury	1.333333	1.333333	2.666667	5.333333

Table 4: Average residual error between model fit and average experimental data				
	4 Hour	14 Hour	24 Hour	48 Hour
Health	0.8406	0.7916	0.7261	1.4567
Injury	1.8826	2.0479	3.695	4.5038

4.5   Individual Parameter Determination

Values for each set of estimated parameters were recorded for each of the individual mice. Presented are the average parameter values for the 5 parameter model, as well as their standard deviations (Figure 17, Figure 18, Table 5). Changes in these

values are reported as percentages, except for the mean of the closing pressures, Pc_μ, are is reported as absolute changes. Because the mean closing pressure in the healthy mice is very close to zero and changes greatly in injury, reporting this as a percentage would somewhat overstate the importance of this change (percentages appeared in the range of 30,000 percent difference). No statistically significant difference in any parameter was reported within the 4 groups of healthy mice. The most pronounced, and only statistically significant parameter change from health to injury was an increase in Pc_μ. As injury severity increased, both the opening and closing pressures progressively increased, though the changes between time points were not statistically significant. Additionally, no statistically significant changes in their separation, ΔP, were seen over time. The rate of opening increased slightly in early injury, but fell to below the control level by 24 and 48 hours. Unexpectedly, no significant differences in the closing and opening velocity constants or the standard deviation of the pressure distributions were seen between any health and injury conditions.

Table 5: Parameter values obtained using the five parameter model
All data shown as mean +/- standard deviation.

Healthy	4Hours	12 hours	24 Hours	48 hours
Pc mean	-0.0548 +/- 0.0202	-0.0454 +/- 0.0162	-0.0440 +/- 0.0162	0.1004 +/- 0.0162
Pc sigma	4.5482 +/- 0.9354	4.2064 +/- 0.9476	3.3816 +/- 0.9476	3.6674 +/- 0.9476
So	0.0314 +/- 0.0058	0.0356 +/- 0.0101	0.0331 +/- 0.0052	0.0383 +/- 0.0093
Sc	0.0050 +/- 0.0013	0.0048 +/- 0.0015	0.0052 +/- 0.0009	0.0052 +/- 0.0007
Delta	4.2370 +/- 1.0995	4.0261 +/- 0.3164	4.3036 +/- 0.5183	4.8257 +/- 1.1213
RMSR	0.8406 +/- 0.2908	0.7916 +/- 0.2730	0.7261 +/- 0.1876	1.4567 +/- 0.6958

Injured	4Hours	12 hours	24 Hours	48 hours
Pc mean	2.8499 +/- 0.6090	3.3885 +/- 1.0205	4.0310 +/- 0.8382	4.5496 +/- 1.3830
Pc sigma	2.7341 +/- 0.3194	2.5305 +/- 0.7017	3.2613 +/- 0.6181	3.6375 +/- 0.9903
So	0.0429 +/- 0.0046	0.0390 +/- 0.0091	0.0287 +/- 0.0065	0.0310 +/- 0.0104
Sc	0.0039 +/- 0.0010	0.0042 +/- 0.0020	0.0039 +/- 0.0015	0.0041 +/- 0.0010
Delta	3.6280 +/- 0.8579	3.5733 +/- 1.2093	3.8060 +/- 0.3944	3.5384 +/- 1.3002
RMSR	1.8826 +/- 0.8393	2.0479 +/- 1.2699	3.6950 +/- 2.2843	4.5038 +/- 3.4652
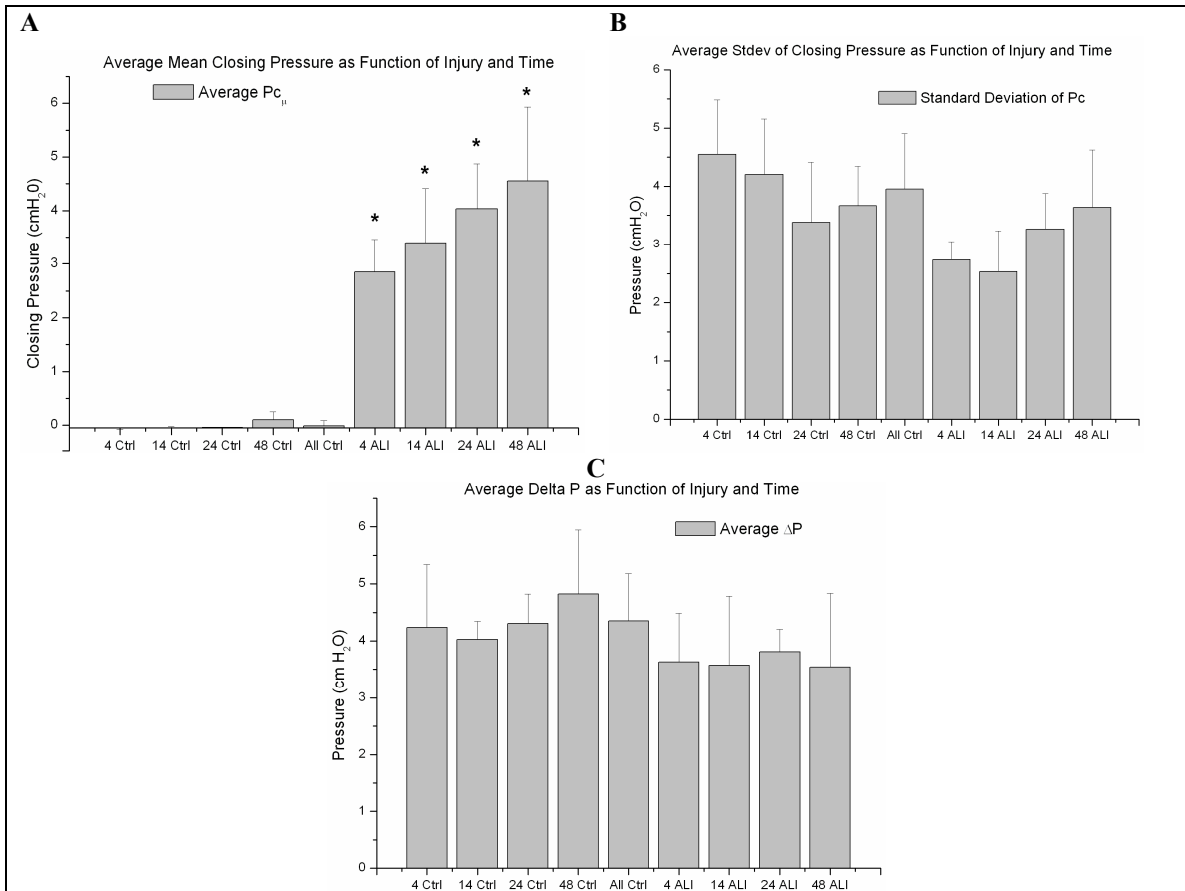
Figure 17: Average parameter values governing pressure distributions for each condition
* denotes statistical significance compared to the all four control groups.
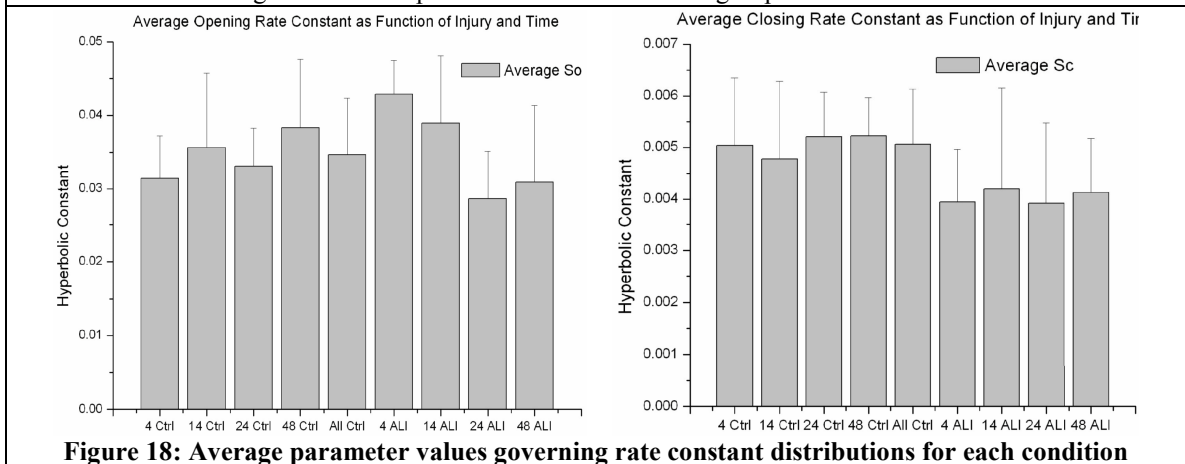
Figure 18: Average parameter values governing rate constant distributions for each condition

4.6 Comparison of Critical Pressure Profiles

Histograms of the distributions of opening and closing velocity slopes for each condition are displayed in Figure 19. Rate constants are displayed using a logarithmic

spacing of bin widths, and plotted semi-logarithmically in x. The y-axis shows the number of airways having in a given bin, normalized per 1000 airways. The distribution of opening and closing slopes for the airways does not significantly change from health to injury, or between injury conditions as it matures. In comparing the opening velocity constant distribution to the closing constants, the opening rates appear to be logarithmically shifted to the right by approximately one decade.

Changes to the average mean and standard deviation of the critical pressure profiles are presented graphically in Figure 20. Panels A and B show the closing and opening pressure distribution generated by the average parameter values for the healthy simulations, while Panels C and D represent the injured mice. In the healthy mice there are no apparent substantial differences among the different time points. Each of the injury time points displays noticeably different pressure profiles from the control, as well as between time points. Initally, the distributions of critical pressures are much more peaked in injury than the control conditions. With increasing injury severity the mean of the distributions continues to increase, as does the width of the pressure distribution.

Figure 19: Distribution of opening and closing Slopes

Figure 20: Average closing and opening pressure distributions
Healthy subjects are shown in the top two graphs, while the injured mice are shown as the bottom plots.
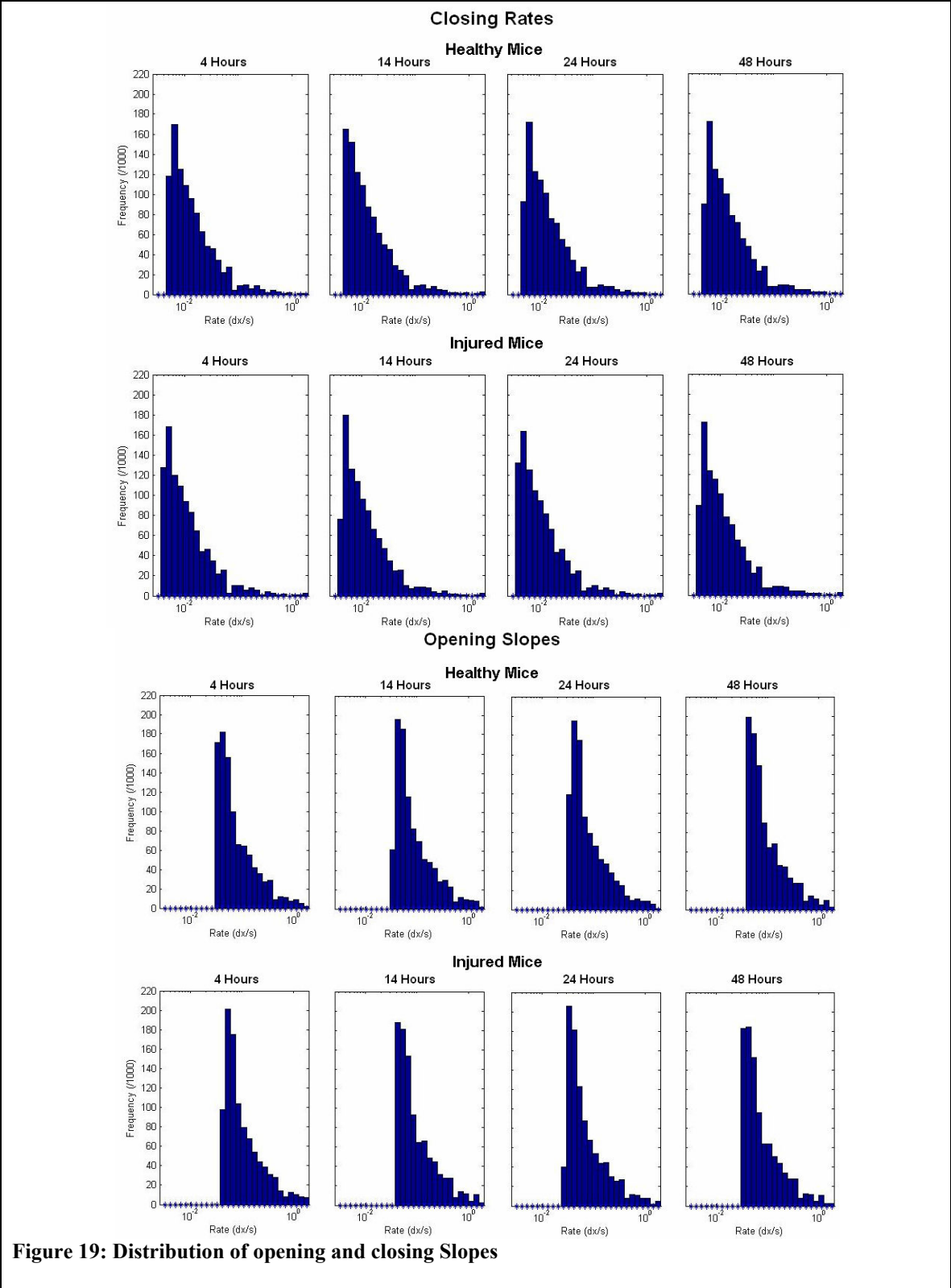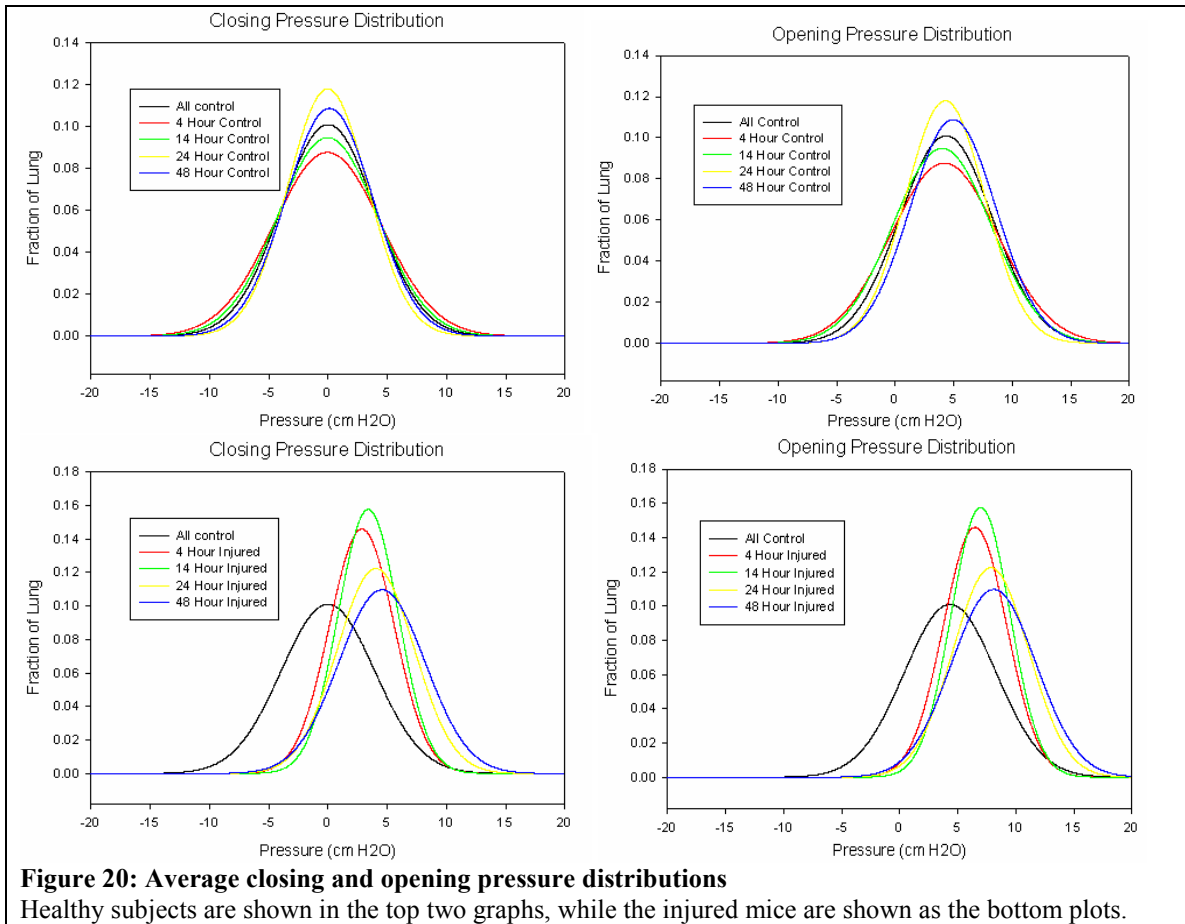
4.7   Sensitivity Analysis

For each individual set of parameters, model sensitivity was measured in both positive and negative directions about the minimum due to potential asymmetry of the parameter space. Average sensitivities were analyzed by experimental condition and are displayed in Figure 21 and Figure 22 as a mean with standard deviation as error bars. The injury condition displayed the most sensitivity to changes in the mean of the closing pressure distribution, while the healthy mice were nearly insensitive to changes in this parameter. By contrast, both the values of *So* and *Sc* had pronounced impact on the fit in the healthy mice, while neither significantly altered goodness of fit in the injured ones.

47

Figure 21: Model sensitivity to changes in pressure distributions

Figure 22: Model sensitivity to changes in distributions of velocity constants
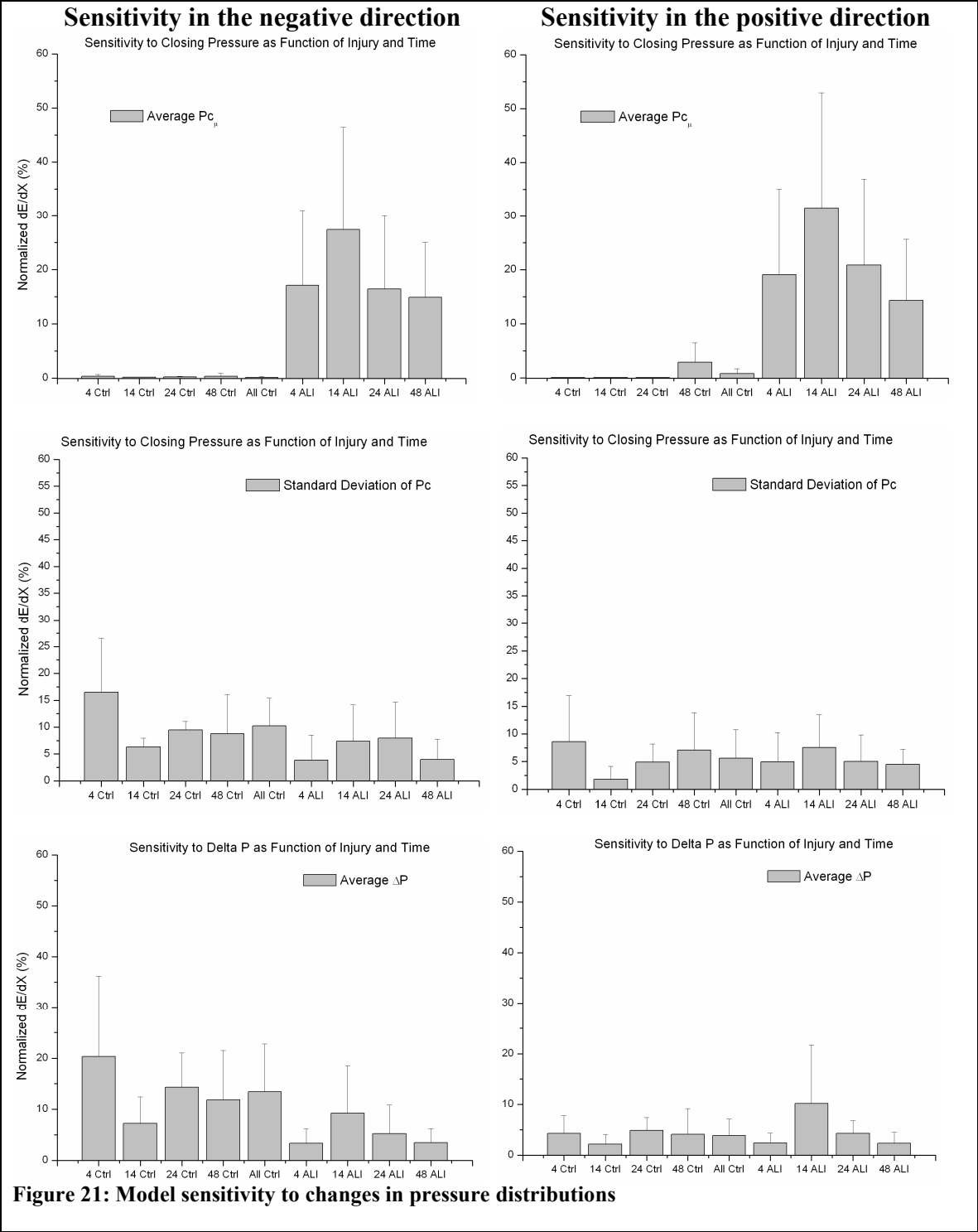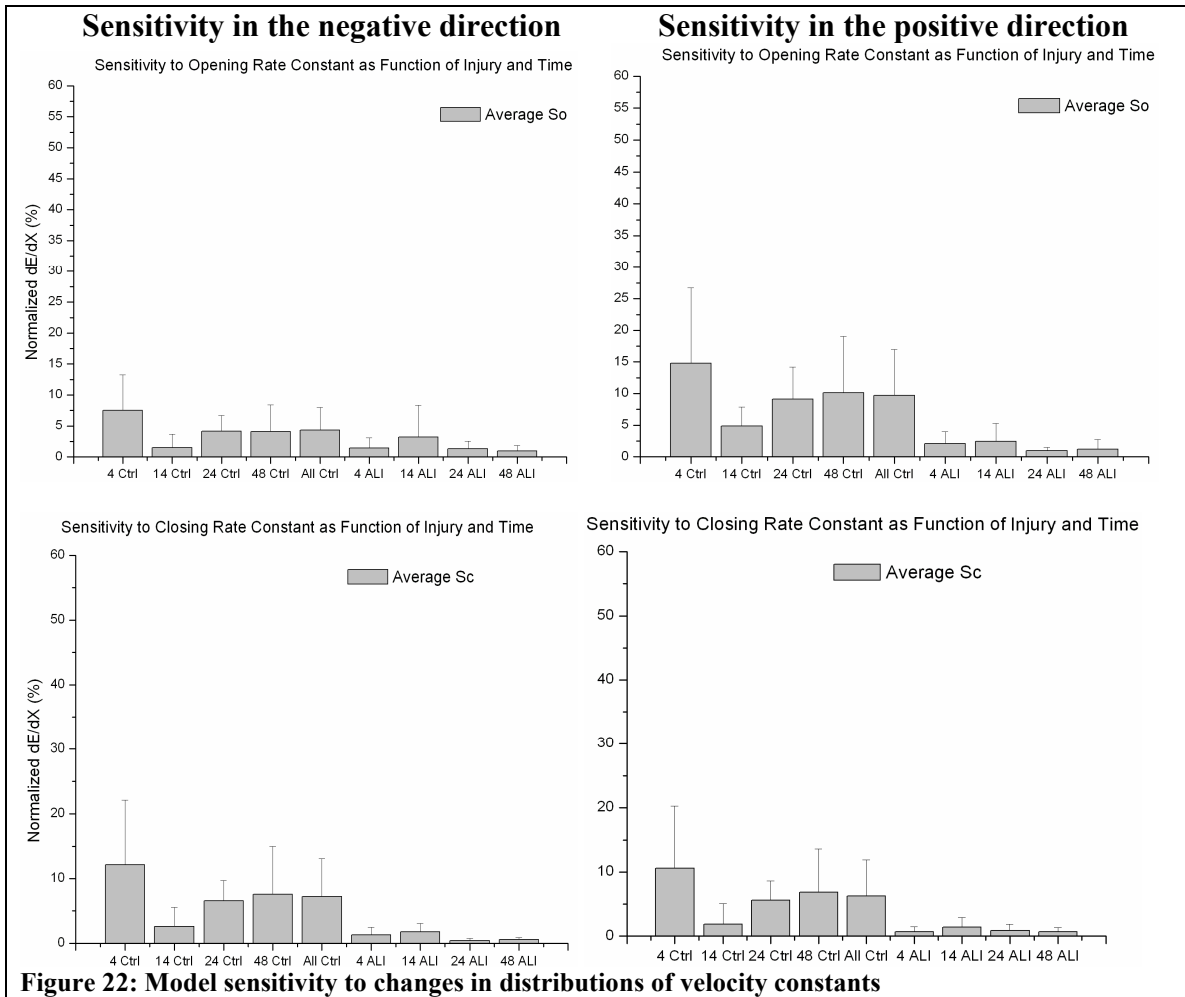
Chapter 5   Discussion

Alterations to the nature of recruitment and derecruitment processes during mechanical ventilation have been implicated in numerous experimental and clinical studies of acute lung injury (3-7, 32, 61). Recent data challenge the long upheld view that recruitment is a static function of pressure in the lung, and rather indicate that this process is inherently dynamic (3-7). As such, lung stiffness can not be viewed simply as a function of pressure, but rather as a function of pressure history and time (9). The clinically relevant implications of this finding on ventilator management are potentially far-reaching, but they have remained bounded by the lack of quantification of specific alterations to the parameters that give rise to dynamic R/D behaviors.

Bates and Irvin proposed the first model of global lung mechanics to incorporate dynamics into the process of airway recruitment and derecruitment (9). Rather than allowing recruitment to be a static function of pressure, this model describes the R/D behavior in the lung by incorporating a nonlinear memory element that stores the impact of pressure history on airway opening or closing. In simulating sinusoidal ventilation, the model mimicked the hysteretic behavior of the Pressure-Volume curve, in particular demonstrating that volume history dramatically affects this relationship by changing the lung's state of recruitment. In allowing the model lung to have particular distributions of closing pressures and closing rates, this model demonstrated a progressive increase in lung stiffness throughout simulated ventilation, similar to dynamic collapse seen in acute lung injury.

The goal of our study was to extend the model of Bates and Irvin to determine distributions of parameters governing R/D phenomena in healthy mice, as well as to

characterize specific alterations to these distributions that occur during states of acute lung injury. To achieve such a goal we tested several potential model architectures that deviate from the original model to identify the model that best characterized the data for parameter estimation. To the best of our knowledge, our model is the first to precisely recreate the transient response of lung elastance following deep inflation. In modeling this phenomenon we have provided the first quantitative description of dynamic R/D parameters that give rise to the complex behavior seen in ALI. We believe these data to be an invaluable prerequisite to future experimental and theoretical evaluation of the safety and efficacy of ventilation strategies.

5.1   Interpretation and Significance of Results

Several modeling studies (22, 26, 27, 35, 36) have previously indicated that a separation of opening and closing pressures gives rise to the hysteresis of the pressure-volume relationship during a ventilatory cycle. By incorporating a memory element that accounts for the role of pressure history in recruitment, Bates and Irvin (9) demonstrated that such hysteretic behavior could also be recreated if the rates of opening and closing processes were separated, while the closing pressure was equal to the opening pressure. In light of this, it was essential to determine whether one or both of these mechanisms contribute significantly to the dynamics of progressive derecruitment. Initially we posed four potential model architectures that link the process of airway recruitment and derecruitment to distributions of opening and closing pressures and rate constants. In fitting each model to the average lung stiffness from experimental data and computing Akaike probabilities on each, we have determined that opening and closing rate constants

must be independent of each other and that a separation of opening and closing pressures is essential to demonstrating the dynamic recruitment and derecruitment behavior seen experimentally. These preliminary model fitting exercises demonstrate that the incorporation of a separation of both pressure and rate quantities is necessary and sufficient to characterize all three prominent features of the experimental data: the initial recovery following deep inflation, the transient recollapse that occurs during ventilation, and the differential response to varying PEEP.

By fitting this model to all of the individual mice we have estimated values for the parameters that govern the dynamics of R/D. By averaging the parameter values over all mice in each condition we have obtained means and standard deviations on each of the parameters, allowing direct comparison between experimental conditions. Interestingly, the only statistically significant changes that occur between health and disease are a parallel increase in both the mean of the critical closing pressure and the mean of the opening pressure. The opening and closing pressures increase progressively with injury severity, though the changes between injury conditions are not statistically significant. In examining the distributions of opening and closing pressures it is clear that the pressure dependence of recruitment is significantly altered in disease. Early in the course of injury the pressure distributions are significantly narrowed compared to the control mice, however the width of the distributions grows as injury progresses. In injured states, a significant portion of the lung has closing pressures that are experienced during tidal ventilation making the injured lung more prone to spontaneous collapse. Additionally, the pressure required to reopen these airways is increased, making recruitment significantly more challenging and potentially more injurious. No change was observed

between health and injury to either the values of *So* and *Sc* or the ultimate appearance of the distributions of these velocity constants. Our analysis shows that the distributions of rate constants for the opening process are inherently faster than those governing closing, with the entire histogram logarithmically shifted to the right by nearly a decade.

Review of the literature suggests that the alterations to recruitment parameters estimated by our model are best explained mechanistically by an inactivation of respiratory surfactant. Several studies (45, 52, 53, 66) have indicated that airway opening pressures increase substantially with surfactant inactivation-mediated increases in surface tension. In contrast, the rate of reopening once this yield pressure is exceeded was found to be dramatically affected by changes to the viscosity of airway lining fluid, but was insensitive to changes in surface tension (52). This suggests that alteration in mucus production is not a significant determinant of altered reopening behavior in this experimental model of acute lung injury. We therefore conclude that increased surface tension is responsible for the increases in airway opening pressures seen experimentally.

To test the validity of this conclusion we compared the opening pressures estimated using our computational model with those predicted on theoretical grounds for small airways (see Appendix). To do this we balanced the pressure, viscous and surface tension induced stresses at an air-liquid interface in a circular airway with a radius of 0.2 mm. We have calculated a theoretical value of 7 cmH2O for the opening pressure which is similar to the values predicted by our model (4.0 cm H_2O in healthy mice to 8.0 cm H_2O in the lung injured mice). The Capillary number for this system (Ca $\sim 2.00 \times 10^{-4}$) also indicates that interfacial behavior in an airway of this size is significantly more determined by surface tension than viscosity. These observations strongly agree with our

conclusion that altered surface tension, presumably through surfactant dysfunction, is responsible for the change in airway reopening behaviors seen in injury.

Increases in opening pressures during injury may be a significant mechanism by which cellular injury occurs in ventilator induced ALI. Studies of moving air bubbles over cultured pulmonary epithelial cells have demonstrated that injury is caused by the steep normal pressure gradient located at the front of the moving finger of air (11). Increases in the yield pressure required to initiate reopening is expected to dramatically increase the magnitude of the pressure gradient established before bubble propagation. Damage to the epithelial layer was completely ablated by the addition of synthetic pulmonary surfactant to the system, through a reduction of the interfacial pressure gradient (11). Pressure gradient magnitude is inversely related to the capillary number in this system, which indicates that cellular injury decreases with increases in *Ca.* Injury is thus worsened by increased surface tension and decreases in fluid viscosity or reopening velocity. Several studies (11, 43, 65) have demonstrated that cultured pulmonary epithelial cells are considerably more prone to death during slow as opposed to fast reopening processes. This observation may be especially worrisome clinically, given that our model predicts an increase in surface tension and, potentially, a decrease in opening velocity, since the pressure differential driving the rate of reopening (not the same as the normal pressure gradient causing injury) will have fallen in injury, while the rate constant remains the same. Another concern from these studies arises from the observation that repeated exposure to pressure fronts that appear initially to be sub-injurious have been shown to cause cumulative injury that increases with the number of insults (43, 65). This

underscores the need for effective recruitment that does not allow for repeated closure and reopening during ventilation.

Though the biophysics literature has more thoroughly characterized reopening phenomena, the majority of the behavior seen in the experiments we have modeled is that of progressive collapse. Evidence suggests that the increase in closing pressures also results from surfactant inactivation mediated increases in surface tension (14, 33, 50). Studies performed in rigid tubes have demonstrated that fluid instabilities spontaneously arise in annular geometries where a thin film coats the walls and an immiscible fluid of different density fills the core of the tube (14). The rate of development of spontaneous collapse is dependent on the film thickness, ε, and surface tension, γ. In a non-rigid tube, collapse appears to result from fluid-elastic instabilities during wave propagation, whereby surfactant driven thin film motion deforms the boundaries of the airway wall, resulting in closure if outward-directed elastic forces are overcome. Collapse of compliant airways appears to result from this fluid-elastic instability secondary to the amplification of fluid waves (33), though peripheral airways may act more like rigid tubes due to mechanical support from the parenchyma (14). Which mechanism predominates in injury remains unknown, however the importance of film thickness in both cases is similar. Surfactant inactivation has been attributed to a decrease in the threshold film thickness, ε_c, above which liquid bridges will form, resulting in incrased airway closure. One study performed in elastic tubes noted that addition of surfactant to a model airway system resulted in a 60% reduction in ε_c and five-fold increase in the duration of patency before collapse occurs (33). This alteration to the rate of collapse may appear paradoxical to the conclusions of our study; however, the rate of collapse

must be thought of as the product of the airway's closing rate constant and the gradient between applied and critical pressure. In the presence of increased closing pressures the pressure differential driving airway instability decreases, given that applied pressure remains the same. This in turn reduces the rate of airway closure independent of changes to the rate constant.

Visualization of the rate constant histograms show that the entire distribution of opening rate constants is ten-fold faster than the distribution of closing pressures and unchanging between health and injury. This disparity is most simply explained by a mechanistic difference between the processes of airway opening and closing: closing is related to either stable fluid meniscus formation or fluid-elastic instability, while reopening is governed by the kinetics of driving a bubble of air through some closed region. Also, axial support from parenchymal tethering forces acts in opposition to the closing of an airway, which may retard the rate of collapse. Interestingly, the inherent rates of both opening and closing processes appear invariant between health and disease even though the pressure dependence has been altered, arguing against the significance of parenchymal tethering since fluid extravasation into the lung tissue during early ALI as well as fibrin accumulation in late injury would both be expected to alter the apparent contribution of parenchymal tethering forces. In summary, our rate constant data can neither provide explicit support nor refutation for either the theory of closure through liquid bridge formation or compliant collapse with structural deformation.

Our sensitivity analysis reveals significant differences in model sensitivity to the mean of the closing pressure distribution. In the injured mice, the data are clearly best characterized by the value of Pc_μ, while the healthy mice are least sensitive to changes in

this variable. We have examined the possibility that this may be an artifact of the normalization used in computing $d\Phi/dX$ for the critical closing pressure. Since we have used an absolute, rather than percent change, to the value of Pc_μ and then subsequently normalized to this change, the denominator of this sensitivity measure may be biased by the relative difference in the parameter change between healthy to diseased condition. In order to determine the impact that this effect would have on the sensitivity measure, we computed $d\Phi/dX$ for various magnitudes of ΔPc_μ and found that the variability in the normalized sensitivity measurement changed no more than ~7% in all conditions, using reasonably small perturbations. Given these simulations, the relative insensitivity to the opening pressure in healthy mice is likely not due to computational artifact. Another more satisfying explanation for this observation is that such a large portion of the healthy lung is above the closing pressure, especially at the higher levels of PEEP, that slightly shifting Pc_μ results in only a small fraction of the lung moving to a state where it can collapse. Paradoxically, this slight increase in collapse may in turn increase airway pressures so that a similar fraction of the lung is now above its (slightly lower) opening pressure, causing the model elastances to change only slightly. The opposite effect may be a sufficient explanation for the sensitivity to this parameter in the injured mice; since so many of the lung's airways are above this closing capacity at various levels of PEEP incremental changes can dramatically influence the goodness of fit. Sensitivity to all other parameters was comparable between groups and no statistically significant differences were observed.

5.2 Critical Appraisal and Model Limitations

In order to employ the R/D paradigm within our simulations several modifications to the work of Bates and Irvin became necessary. Our first modification to the model was the departure from the Salazar and Knowles equation (54) to describe peripheral lung mechanics and the adoption of the single compartment model for each unit. Use of a parallel arrangement of single compartment units allows the whole lung resistance and elastance to vary inversely with the state of airway recruitment. This also allows the airway motion equations to be explicit in volume, flow and pressure, as opposed to relating volume to pressure alone. This change facilitates the conservation of flow during ventilation. The downside to using our model over Salazar and Knowles is that the peripheral mechanical elements do not exhibit an increase in elastance due to strain stiffening behavior demonstrated in lung tissue at higher volumes. Though the significance of this effect has not been examined, we believe that the effect of recruitment and derecruitment would likely predominate over strain stiffening in these conditions, though incorporation of tissue mechanical properties that are nonlinear functions of volume is a logical extension of our analysis.

In coupling the lung model with an implementation of the ventilator we have allowed for the resistance and gas compression occurring within the experimental equipment to be accommodated for directly. The current ventilator paradigm is hard-coded into the model, requiring modification to the current programs in order to simulate ventilation strategies that significantly differ from the current approach. In particular changes to the ventilation frequency or the length of the interval between measurements will require an alteration of the sampling rate and window length in order to avoid the

virtual-auto PEEP problem mentioned in the methods section. A method of directly

visualizing the impact of these changes on the pressure, volume and flow waveforms over

several breaths has been incorporated into the code so that values for the sample rate and

window length can be chosen to appropriately meet user defined design criteria. The

windowed approach to data storage in 15 second parcels was originally employed to

minimize the amount of data required for storage, by replacing it after each measurement

interval. The current implementation of the model can easily be modified to remove this

windowed approach to simulating the data in favor of some other data structure that is

less sensitive to these timing variables.

Our current method of determining the value of respiratory elastance is

determined by fitting the equation of motion for the single compartment model to the

pressure, volume and flow tracings from the model. At present the curve fitting is

accomplished with the Levenberg-Marquardt algorithm using end expiratory R_L and E_L

for initial guesses. This curve fitting approach was chosen for determination of E_L, as it

was initially unclear which was the best equation to characterize the effective elastance.

Since the equation of motion for the single compartment is linear in both R and E, this

approach to parameter estimation is unnecessarily intense compared to solving a simple

linear least squares problem with a simple matrix inversion operation in Matlab. Despite

this, Matlab's code profiler only attributes 0.7% of the simulation time to the estimation

of E_L. In fact, an estimate of average E_L may even be obtained by taking an average of

the value for E_L over a few breaths every 15 seconds of ventilation based on the number

of open lung units. It is presently unknown how well this measure would compare with

59

the effective elastance of the respiratory system calculated by curve fitting. Since the model is linear and subject to similar assumptions, a very good agreement is expected.

Our final model uses 1,250 terminal airways to recreate the recruitment/derecruitment behavior seen experimentally. In preliminary studies fitting the four potential models to the average elastances we initially used 2,500 airways. Once the model fitting was completed we compared the goodness of fit and the elastance time-courses to additional simulations performed with 500, 750, 1250, 2000 and 5000 airways. The model fit was nearly invariant to all of the potential choices of airway numbers listed above, except for the 500 airway case in which the trend in the data was the same, but the elastance tracings became slightly more jagged, with approximately 5% increase in error.

One of the most important factors affecting the behavior of the model is the tidal volume that it is driven with. Estimates of parameters were found to change significantly if the tidal volume of the model was varied. This is not a practical issue in our simulations since the target volume displacement is known for these measurements. It should be considered when comparing the distributions generated in these simulations to those from other experimental data that may be conducted at other tidal volumes. Of lesser importance than tidal volume, but still of potentially significant consequence is the model sensitivity to the value of E_{unit}. Changing the value of E_{unit} by 5% with all other parameters held constant caused an increase in the error of 60-80%, depending on the injury condition. Interestingly, fairly small changes to E_{unit}, on the order of 1%, actually caused a slight decrease (~7.5%) in the model error. We had chosen the value of 22 cmH$_2$O for E_L of the fully open lung, which is slightly lower than the elastance of the healthy mouse lung measured 15 seconds after deep inflation. The figure we used was

chosen below the measured value as there is likely to have been some collapse that occurs during this time period, as well as the potential for incomplete recruitment in response to the DI. Simulations have not been performed where model parameters are fit with varying values of tissue elastance. It would, however, be interesting to quantify the precise impact this has on model parameters. Since tidal volume is such a strong determinant of these estimates, the relative importance of tissue elastance, or its coupling with tidal volume should be examined, as these sensitivities were incompletely explored.

Though a normal distribution of critical pressures has been widely reported in the literature (15, 28, 35, 36, 51), the true underlying distribution of these quantities is more than likely not perfectly Gaussian. We have also performed simulations whereby the distribution of opening and closing pressures are distributed log-normally; however, these yielded roughly 2-2.5 fold higher errors than the normally distributed case (data not shown). This increase in error may be due in part to the limitations of using only a scale and shift parameter to determine the shape of the log normal distribution, as the shape parameter will unpredictably effect the mean, standard deviation, kurtosis and skewness of the distribution. A more controllable implementation of this distribution may be generated by shifting and scaling a Gaussian distribution and then projecting it into log-space using a Jacobian transformation. Some simulations fitting the log-normal distributions of critical pressures resulted in negative values for ΔP, which are counterintuitive and presumably non-physiologic. The possibility exists that this results from finding a local minimum that may be avoided by using a constrained optimization algorithm that requires ΔP to be positive. Previous studies have also posed that the opening pressures may be uniformly distributed. This was felt unlikely to be a realistic

distribution in our model, as most of the models that use the uniform distribution generally incorporate branching in the airway tree and simulate cascades of progressive airway opening (55-58). Increasing model complexity by incorporating additional airway branching and the potential for serial collapse and reopening is scientifically relevant and may be an area for future exploration. As an early simulation of this recruitment/derecruitment paradigm, we avoided this degree of complication and were able to successfully characterize the experimental data with a minimal number of free parameters. Early simulations were performed with both hyperbolic and uniform distributions of So and Sc; however, simulations with the uniform distributions were found not to converge to reasonable elastance time courses. In general, future studies applying this model to other experimental data sets may benefit from simulation with these alternative distributions of pressures and rate constants, as the behavior in other experimental conditions may be better approximated this way.

In the absence of any firm evidence in the literature that provides a functional relationship between opening and closing pressures we elected to begin with a constant separation of these quantities. Though the incorporation of a separation of airway opening and closing pressures was instrumental in fitting the model to the data, we have no reason to believe that a point estimate of the separation would characterize the biophysics better than some non-zero variance formulation. We have therefore examined simulations where the critical pressure separation has an additional degree of freedom; however, this was not found to improve the model fit. In allowing the distribution of ΔP to be distributed uniformly on $[0, \Delta P_{max}]$ there was an increase in the residual error of the model, indicating that this particular distribution did not appropriately reflect the

separation between opening and closing pressures. That is not to say that some other distribution of pressure separations would not fit the data better. In fact, increasing the number of free parameters would be expected to decrease the residual error (provided the models are nested). Using some distribution of opening pressures, for example a uniform distribution on $[\Delta P_{min}, \Delta P_{max}]$, may increase the goodness of fit, but the cost of the additional free parameter may not be justified. Similarly, allowing for the standard deviation of the opening distribution to vary independently of the closing distribution may cause a reduction in residual error. It should be noted again that our results describe distributions in this particular injury condition in one species and are not directly generalizable beyond this case without outside validation by testing potential model variants as appropriate.

Alternative approaches to the Nelder and Mead Simplex algorithm (46) were examined for fitting the model to the data. One advantage of using a search algorithm is that it requires only calls to the model function during an iteration, as opposed to having to numerically calculate derivatives of the cost function. Though a closed form analytic expression may conceivably exist for the model's partial derivatives, the dependence of the initial mechanical state of the model after deep inflation on the model parameters significantly complicates the determination of such a solution. A higher order optimization scheme would thus require using numerical estimates of first and second order partial derivatives for generation of components of the Gradient and Hessian matrices. This strategy was not attempted because it was felt it would require far greater computational time to compute these matrices without increasing the robustness of the approach.

Another concern regarding the approach to fitting the model regards the need to determine with high certainty that the optimal solution is in fact a global, rather than local minimum. Though we are confident we have obtained the correct physiologically bounded solutions, the need to ensure convergence to the physiologic global minimum in medical-grade technological applications can not be understated, so that clinical decisions are based on the appropriate values. Investigation of algorithms that can more effectively span the parameter space for other physiologically relevant minima may be a worthwhile venture. A significant downside to application of global optimization routines is the increase in the number of iterations required for a solution to be reached. The typical termination criterion for this approach is to accept the set of parameters generating the lowest error after a predetermined number of iterations is reached. This introduces the problem of not assuring convergence, as the user defined number of iterations is considered a weak criterion for termination. If convergence needs to be assured, any traditional optimization technique may be used about the "minimum" found by the global technique.

Two methods worth mentioning for global optimization are the Simulated Annealing (44) technique and Evolutionary Optimization using Genetic Algorithms (17, 19, 21). In contrast to traditional optimization strategies, where only decreases in residual error are accepted and considered as moving closer to the desired minimum, these strategies will elect to introduce some iterations that increase the model error, occasionally moving the model away from the neighborhood of a local minimum and allowing it to search for a new optimal solution. The search operation used in Simulated Annealing (SA) adds a perturbation to the parameter vector whose magnitude and

direction is based on a point chosen at random on the surface of an L-dimensional unit hypersphere. After evaluating the function at the new parameter set, it determines if the error has been reduced. If error has decreased, the step is always accepted; however, if there is an increase in error a probabability of acceptance that is inversely related to the magnitude of the error is calculated. A uniform random number is chosen on the interval [0,1] and compared to the acceptance probability: if the random number is less than the acceptance probability, this step is retained, otherwise the algorithm rejects this change and reverts to the previous value. Genetic algorithms use the natural processes of recombination and natural selection to evaluate the model at permutations of tested solutions (19). The process begins with a population of several proposed optimal solutions – or design vectors - which it evaluates before subjecting them to evolutionary operations. Several potential operations can be performed, including breeding pairs of solution vectors to generate new "child" design vectors, and random mutation by the addition of spontaneous perturbation to certain solution components. The introduction of randomly generated "immigrant" solutions to the population generates new design vectors unrelated to the initial population. The new population of parameters from the children, mutants and immigrants can increase the diversity in potential solutions by spanning large regions of parameter space. The genetic algorithm evaluates the function at each member of the population and uses the residual error to whittle down the possible solutions by only accepting the best few parameter sets. Iteration of this algorithm over time reduces the presence of weak parameter values that poorly characterize the data, eventually reaching the neighborhood of an optimal solution.

The primary limitation which prohibits clinical use is the long duration of the fitting process. Currently, one iteration of this model takes approximately 28 seconds of computational time. At roughly 200-250 function calls required for convergence, one fitting routine takes approximately 2 hours to complete. This delay between acquisition and parameter estimates significantly precludes its utility at the bedside, and certainly rules out its application in embedded model control within a ventilator, at least in its present form. Strategies to reduce the computational burden and increase its potential use at the bedside are discussed in greater detail below.

5.3   Model Utility and Future Directions

The observation that mechanical changes in ALI can be recreated solely through stochastic collapse supports the recent body of literature arguing against changes in intrinsic tissue mechanical properties as the predominant cause for apparent parenchymal stiffening. The pressure and rate constant distributions generated by our fitting exercise provide quantification of the precise derangement to recruitment behaviors seen in acid induced lung injury. This provides insight into both the biophysics of R/D in this particular injury model, as well as a conceptual basis for future advances in design of ventilator protocols. To this end, the computational model has potential utility in studying other types of experimental lung injury, differential response to injury in different strains of mice or different organisms and future adaptation for clinical application.

Applying the same model in mice with lung injury of differing etiology may shed light on mechanical differences between pathologies at the airway level. Comparison of

the experimental data used in our study with a saline lavage injury from an earlier study in our lab (4) demonstrates a significant difference in response to recruitment maneuvers, as well as the extent and rapidity of derecruitment. It is particularly relevant to compare the derangements to R/D phemonena in different models of ALI as significant debate exists about the extent and impact of heterogeneity in the patient population on appropriate management strategies (28, 29, 47, 48, 63). Specific alterations to recruitment processes in various injuries should be quantified by fitting to experimental data where the identical ventilator protocol is used following saline lavage (drowning model), simulated fat emboli-syndrome with oleic acid exposure, nebulized endotoxin exposure or experimental sepsis with mechanical ventilation following cecal puncture. Another potential use for the model is to examine the differential effects of acid instillation in the same ventilator protocol in other mouse strains or in other model species. Similarly, the effect of various pharmacologic agents could be evaluated in terms of their effect on altering R/D behaviors. In comparing experimental studies it may be an important consideration to use the same ventilator protocol, as there is synergy between the injury caused by the primary insult and the mechanical stresses that cause ventilator induced lung injury (VILI).

This model in its current form may be less than ideal in studying pure VILI that results solely from parenchymal overdistension at high tidal volumes or the excessive shear injury of collapse at low PEEP. In these situations, high mechanical stresses cause an injury that is progressive during the data collection period. Fitting this model to the entirety of the data would lump progressive mechanical alterations together, averaging over the incremental changes that occur over relatively short time scales. A compromise

may be to fit the model sequentially to overlapping windows of the data and estimate how VILI changes the estimates of parameter values over time, using the parameter estimates of the previous window as the next window's initial guess.

In order to further increase the utility of this model, some quantification of the injurious nature of mechanical ventilation should be sought. Given that the distributions of R/D properties are now known for healthy and injured mice, some quantitative measure that correlates with injury severity can be posed for the assessment and optimization of ventilation in each condition. This injury function should account for the impact of parenchymal overdistention, regional collapse and cyclic reopening and closing; however, the relative importance of each processes in promoting injury are unknown. The mathematical form of the injury function can be tested and validated by assessing it in each measurement period and ensuring that it correlates with other established measures of injury severity from the experiment. Differing injury conditions, such as those outlined above could be assessed objectively to quantitatively determine the extent of injury experienced in various experimental models. Additionally, biochemical or physiologic markers of injury may be correlated with levels of tissue stress in the model, which may help identify measurable candidate biomarkers that correlate with our index of injury severity.

Establishing a reliable function to quantify the extent of injury given distributions of recruitment and derecruitment parameters allows for several areas of model exploration. One potential application is in the determination of optimal tidal volume and PEEP in conventional ventilation by minimization of the injury cost function. Additionally, optimal settings for conventional ventilation may be compared with other

experimental techniques, such as variable tidal volume ventilation, whereby the amplitude of V_T varies probabilistically between breaths. Potential optimal ventilator strategies may subsequently be validated *in-vivo* by comparison of each strategy for efficacy and correlation with biochemical and mechanical measures of injury severity. Of particular interest is the assessment of how well the dynamics of mechanical changes compare to the model prediction. These combined experimental / model / optimization studies, if successful in animals, may demonstrate potential utility in the clinical management of human patients in the intensive care unit.

In its present implementation, the model takes far too much time to be used directly in any kind of embedded, model-based ventilator control or on-line, dynamic assessment of lung mechanics in intensive care patients. The first necessary adaptation that will hasten its use in a direct clinical application would be to transition to a compiled programming language capable of interfacing with clinical hardware. It is expected that using a compiled language will significantly reduce the computational time per iteration. Using the Matlab Profiler we have determined that 97% of the simulation time is determined by the length of the protocol and the sample rate, not the number of elastance estimates made. One advantage of moving to a human patient is that breathing frequency decreases and the sample rate can be reduced significantly below 60 Hz, which lessens the number of points required for simulation. Preliminary simulations will have to be run with human respiratory parameters to determine an acceptable simulation rate. Another way to increase the speed of the model is to construct a diagnostic ventilator waveform designed to produce optimized information for the purpose of fitting our model. At present, the design criteria for such a waveform are unknown, but should consist of

perturbations that take into account the immediate and transient response to deep inflation, as well as the recruitment response to PEEP. By measuring lung mechanics more frequently, the model may be able to fit a larger volume of data with more pertinent information at reduced simulation time. Eventually, the predictions of parameter distributions at the bedside may be used in embedded model control of ventilation, by dynamically optimizing ventilator parameters that reduce the injury potential of a ventilator strategy.

Several modeling concerns arise when considering the use of this model in humans, especially intensive care patients. One shortcoming of this model is that it may not accurately simulate the elastance time courses of larger animals with considerably more rigid chest cavities. Incorporation of a chest compliance element in series with the lung is essential to the application of this model to analysis of human data, especially in certain chest pathologies or under the influence of pharmacologic sedation/paralysis both of which increase the rigidity of the chest wall. Nonlinearities introduced by the endotracheal tube or expiratory flow limitation may alter the estimates of respiratory parameters and should be entertained when considering determining mechanics from the ICU patient, especially given the potential sensitivity to the value of tissue stiffness used in the model.

Another concern arises with regard to the patient on ventilatory assist, whereby respiratory function is partially supported, but not controlled by the mechanical ventilator. In these patients, identifying a waveform to drive the model lung for parameter estimation and the eventual prediction of ventilation efficacy becomes nearly impossible, as the pressures the model will generate are a function of the model's state of

recruitment. There may be several potential ways around this issue, including placing a pneumotachometer within the ventilator circuit and fitting the model to measured pressure and flow rather than estimated elastance, though the practical complications arising from such a venture may outweigh the information garnished by this approach. Another complicating factor comes from the difficulty in determining lung volume, and its resulting contribution to lung mechanics. Reliably estimating this quantity, especially in the face of pathology, adds another level of complexity to an already difficult clinical engineering problem. If these shortcomings could be reasonably overcome, a modeling approach similar to ours would have great value in predicting optimal settings for the patient on ventilatory support, particularly in Airway Pressure Release Ventilation (APRV), where patients breathe freely over high levels of static pressure with periodic "exhalations" to a lower PEEP in order to clear CO_2. Our modeling could be used to identify optimal high and low pressures and the transition timing that will allow spontaneous ventilation over a pressure range that is both minimally injurious and comfortable in the awake patient.   Optimized APRV that adapts to the patient's state of recruitment may even be an ideal strategy for weaning ventilator dependant patients off mechanical ventilation.

Chapter 6   Conclusions

In this study we examined the quantitative nature of how airway recruitment and derecruitment behaviors change during acute lung injury. Through simulation of stochastic airway collapse we have recreated the time course of elastance changes seen in experimentally ventilated mice. In fitting various models to the data, we have determined that opening and closing rate constants must be independently distributed, while the opening and closing pressures must not be equal in order for the model to capture all relevant features of recruitment and progressive collapse. Using this insight, we have estimated values of parameters governing R/D phenomena and determined that a parallel increase in airway opening and closing pressures is responsible for impaired recruitment seen in ALI. It appears as though these increases in both critical pressures are progressive as injury matures, though the finding is not statistically significant. These observations point toward surfactant deactivation rather than mucous plugging as the likely mechanism by which derecruitment is exacerbated.

Optimization of lung recruitment in the intensive care unit must take into account the dynamic nature of stochastic airway derecruitment. Characterization of the distributions of pressure and rate constants that govern this behavior is an invaluable precursor to the design and assessment of novel ventilator strategies in intensive care. In quantifying parameters governing these distributions we provide data that can be incorporated into novel forward-simulations for evaluation and optimization of ventilation, in particular, recruitment maneuvers, PEEP and variable tidal volume ventilation.

References

1.   **Acute Respiratory Distress Syndrome Network**. Ventilation with lower tidal volumes as compared with traditional tidal volumes for acute lung injury and the acute respiratory distress syndrome. *The New England Journal of Medicine* 342: 1301-1308, 2000.

2.   **Akaike H**. A new look at the statistical model identification. *IEEE Transactions on Automatic Control* 19: 716-723, 1974.

3.   **Allen G, and Bates JHT**. Dynamic mechanical consequences of deep inflation in mice depend on type and degree of lung injury. *J Appl Physiol* 96: 293-300, 2004.

4.   **Allen G, Lundblad LKA, Parsons P, and Bates JHT**. Transient mechanical benefits of a deep inflation in the injured mouse lung. *J Appl Physiol* 93: 1709-1715, 2002.

5.   **Allen GB, Leclair T, Cloutier M, Thompson-Figueroa J, and Bates JHT**. The response to recruitment worsens with progression of lung injury and fibrin accumulation in a mouse model of acid aspiration. *Am J Physiol Lung Cell Mol Physiol* 292: L1580-1589, 2007.

6.   **Allen GB, Pavone LA, DiRocco JD, Bates JHT, and Nieman GF**. Pulmonary impedance and alveolar instability during injurious ventilation in rats. *J Appl Physiol* 99: 723-730, 2005.

7.   **Allen GB, Suratt BT, Rinaldi L, Petty JM, and Bates JHT**. Choosing the frequency of deep inflation in mice: balancing recruitment against ventilator-induced lung injury. *Am J Physiol Lung Cell Mol Physiol* 291: L710-717, 2006.

8.   **Avriel M**. *Nonlinear Programming: Analysis and Methods*. Dover Publishing, 2003.

9.   **Bates JHT, and Irvin CG**. Time dependence of recruitment and derecruitment in the lung: a theoretical model. *J Appl Physiol* 93: 705-713, 2002.

10.   **Bertram C, and Gaver DP**. Biofluid Mechanics of the Respiratory System. *Ann Biomed Engr* 33: 1681-1688, 2005.

11.   **Bilek AM, Dee KC, and Gaver DP, III**. Mechanisms of surface-tension-induced epithelial cell damage in a model of pulmonary airway reopening. *J Appl Physiol* 94: 770-783, 2003.

12.   **Brower RG, Lanken PN, MacIntyre N, Matthay MA, Morris A, Ancukiewicz M, Schoenfeld D, Thompson BT, and National Heart, Lung and Blood Institute ARDS Clinical Trials Network**. Higher versus lower positive end-expiratory pressures in patients with the acute respiratory distress syndrome. *The New England Journal of Medicine* 351: 327-336, 2004.

13.   **Burnham KP, and Anderson DR**. *Model Selection and Multimodel Inference: A Practical-Theoretic Approach*. Springer-Verlag, 2002.

14.   **Cassidy KJ, Halpern D, Ressler BG, and Grotberg JB**. Surfactant effects in model airway closure experiments. *J Appl Physiol* 87: 415-427, 1999.

15.   **Cheng W, DeLong DS, Franz GN, Petsonk EL, and Frazer DG**. Contribution of opening and closing of lung units to lung hysteresis. *Respir Physiol* 102: 205-215, 1995.

16.   **Cheng W, DeLong DS, Franz GN, Petsonk EL, and Frazer DG**. Discountinuous lung sounds and hysteresis in control and Tween 20-rinsed excised rat lungs. *Respir Physiol* 117: 131-140, 1999.

17.   **Crosby JL**. *Computer Simulation in Genetics*. London: John Wiley & Sons, 1973.

18.   **Crotti S, Mascheroni D, Caironi P, Pelosi P, Ronzoni G, Mondino M, Marini JJ, and Gattinoni L**. Recruitment and Derecruitment during Acute Respiratory Failure . A Clinical Study. *Am J Respir Crit Care Med* 164: 131-140, 2001.

19.   **Fogel DB**. *Evolutionary Computation: The Fossil Record*. New York: IEEE Press, 1998.

20.   **Frantzeskaki F, Amygdalou A, Rasmussen TR, Vassiliou MP, and Behrakis PK**. Effects of PEEP on inspiratory and expiratory mechanics in adult respiratory distress syndrome. *Respiratory Medicine* 97: 159-166, 2003.

21.   **Fraser A, and Burnell D**. *Computer Models in Genetics*. New York: McGraw-Hill, 1970.

22.   **Frazer DG, and Franz GN**. Trapped gas and lung hysteresis. *Respir Physiol* 46: 237-246, 1981.

23.   **Frazer DG, Smith LD, Brancazio LR, and Weber KC**. Comparison of lung sounds and gas trapping in the study of airway mechanics. *Environ Health Perspect* 66: 25-30, 1986.

24.   **Frazer DG, Stengel P, and Weber KC**. The effect of pulmonary edema on gas trapping in excised rat lungs. *Respir Physiol* 38: 325-333, 1979.

25.   **Frazer DG, Stengel P, and Weber KC**. Meniscus formation in airways of excised rat lungs. *Respir Physiol* 36: 121-129, 1979.

26.   **Frazer DG, and Weber KC**. Trapped air in ventilated excised rat lungs. *J Appl Physiol* 40: 915-922, 1976.

27.   **Frazer DG, and Weber KC**. Trapped gas at maximum lung volume in intact isolated rat lungs. *Respir Physiol* 37: 173-184, 1979.

28.   **Gattinoni L, Caironi P, Pelosi P, and Goodman LR**. What Has Computed Tomography Taught Us about the Acute Respiratory Distress Syndrome? *Am J Respir Crit Care Med* 164: 1701-1711, 2001.

29.   **Gattinoni L, Pelosi P, Suter PM, Pedoto A, Vercesi P, and Lissoni A**. Acute Respiratory Distress Syndrome Caused by Pulmonary and Extrapulmonary Disease *American Journal of Respiratory and Critical Care Medicine* 158(1): 3-11, 1998.

30.   **Gaver DP, Halpbern D, Jensen OE, and Grotberg JB**. The Steady motion of a semi-infinite bubble through a flexible walled channel. *J Fluid Mech* 319: 25-65, 1996.

31.   **Gaver DP, Samsel RW, and Solway J**. The effects of surface tension and viscosity on airway opening. *J Appl Physiol* 69: 74-85, 1990.

32.   **Grasso S, Mascia L, Del Turco M, Malacarne P, Giunta F, Brochard L, Slutsky AS, and Marco Ranieri V**. Effects of Recruiting Maneuvers in Patients with Acute Respiratory Distress Syndrome Ventilated with Protective Ventilatory Strategy. *Anesthesiology* 96: 795-802, 2002.

33.   **Halpern D, and Grotberg JB**. Surfactant effects on fluid-elastic instabilities of liquid-lined flexible tubes: a model of airway closure. *J Biomech Eng* 115: 271-277, 1993.

34. **Hantos Z, Daroczy B, Csendes T, Suki B, and Nagy S**. Modeling of low-frequency pulmonary impedance in dogs. *Journal of Applied Physiology* 68: 1990.

35. **Hickling KG**. Best Compliance during a Decremental, But Not Incremental, Positive End-Expiratory Pressure Trial Is Related to Open-Lung Positive End-Expiratory Pressure . A Mathematical Model of Acute Respiratory Distress Syndrome Lungs. 2001, p. 69-78.

36. **Hickling Keith G**. The Pressure-Volume Curve Is Greatly Modified by Recruitment . A Mathematical Model of ARDS Lungs. 1998, p. 194-202.

37. **Horsfield K, Kemp W, and Phillips S**. An Asymmetrical Model of the airways of the dog lung. *Journal of Applied Physiology* 52: 21-26, 1982.

38. **Ito S, Ingenito EP, Arold SP, Parameswaran H, Tgavalekos NT, Lutchen KR, and Suki B**. Tissue heterogeneity in the mouse lung: effects of elastase treatment. *J Appl Physiol* 97: 204-212, 2004.

39. **Ito S, Lutchen KR, and Suki B**. Effects of heterogeneities on the partitioning of airway and tissue properties in normal mice. *J Appl Physiol* 102: 859-869, 2007.

40. **Kaczka D, Massa C, and Simon B**. Reliability of Estimating Stochastic Lung Tissue Heterogeneity from Pulmonary Impedance Spectra: A Forward-Inverse Modeling Study. *Annals of Biomedical Engineering* 2007.

41. **Kaczka DW, Hager DN, Hawley ML, and Simon BA**. Quantifying Mechanical Heterogeneity in Canine Acute Lung Injury. *Anesthesiology* 103: 306-312, 2005.

42. **Kaczka DW, Ingenito EP, Body SC, Duffy SE, Mentzer SJ, Decamp MM, and Lutchen KR**. Inspiratory lung impedance in COPD: Effects of PEEP and immediate impact of lung volume reduction surgery. *Journal of Applied Physiology* 90: 1833-1841 2001.

43. **Kay SS, Bilek AM, Dee KC, and Gaver DP, III**. Pressure gradient, not exposure duration, determines the extent of epithelial cell damage in a model of pulmonary airway reopening. *J Appl Physiol* 97: 269-276, 2004.

44. **Kirkpatrick S, Gelatt CD, and Vecchi MP**. Optimization by Simulated Annealing. *Science* 220: 671-680, 1983.

45. **Naureckas ET, Dawson CA, Gerber BS, Gaver DP, 3rd, Gerber HL, Linehan JH, Solway J, and Samsel RW**. Airway reopening pressure in isolated rat lungs. *J Appl Physiol* 76: 1372-1377, 1994.

46. **Nelder JA, and Mead R**. A simplex method for function minimization. *T Comp J* vol 7: 308-313, 1965.

47. **Neumann P, Berglund JE, Mondejar EF, Magnusson A, and Hedenstierna G**. Dynamics of lung collapse and recruitment during prolonged breathing in procine lung injury. *J Appl Physiol* 85: 1533-1543, 1998.

48. **Neumann P, Berglund JE, Mondejar EF, Magnusson A, and Hedenstierna G**. Effect of different pressure levels on the dynamics of lung collapse and recruitment in oleic acid induced lung injury. *Am J Respir Crit Care Med* 158: 1636-1543, 1998.

49. **Otis AB, McKerrow CB, Bartlett RA, Mead J, McIlroy MB, Selverstone NJ, and Radford EP**. Mechanical Factors in the distribution of ventilation. *Journal of Applied Physiology* 8: 427-443, 1956.

50. **Otis DR, Jr., Johnson M, Pedley TJ, and Kamm RD**. Role of pulmonary surfactant in airway closure: a computational study. *J Appl Physiol* 75: 1323-1333, 1993.

51.   **Pelosi P, D'Onofrio D, Chiumello D, Paolo SM, Chiara G, Capelozzi VL, Barbas CSV, Chiaranda M, and Gattinoni L**. Pulmonary and extrapulmonary acute respiratory distress syndrome are different. *European Journal of Respiration* 22: 48S - 56S, 2003.

52.   **Perun ML, and Gaver DP**. An experimental model investigation of the opening of a collapsed, untheterhed pulmonary airway. *J Biomech Eng* 117: 245-253, 1995.

53.   **Perun ML, and Gaver DP**. The interaction between airway lining fluid forces and parenchymal tethering during pulmonary airway reopening. *J Appl Physiol* 79: 1717-1728, 1995.

54.   **Salazar E, and Knowles JH**. An analysis of pressure-volume characteristics of the lung. *Journal of Applied Physiology* 19: 97-104, 1964.

55.   **Suki B**. Fluctuations and Power Laws in Pulmonary Physiology. *Am J Respir Crit Care Med* 166: 133-137, 2002.

56.   **Suki B, Alencar AM, Tolnai J, Asztalos T, Petak F, Sujeer MK, Patel K, Patel J, Stanley HE, and Hantos Z**. Size distribution of recruited alveolar volumes in airway reopening. *J Appl Physiol* 89: 2030-2040, 2000.

57.   **Suki B, Andrade JS, Coughlin MF, Stamenović D, Stanley HE, Sujeer M, and Zapperi S**. Mathematical Modeling of the First Inflation of Degassed Lungs. *Annals of Biomedical Engineering* 26: 608-617, 1998.

58.   **Suki B, Barabasi A-L, Hantos Z, Petak F, and Stanley HE**. Avalanches and power-law behaviour in lung inflation. *Nature* 368: 615-618, 1994.

59.   **Suki B, Yuan H, Zhang Q, and Lutchen KR**. Partitioning of lung tissue response and inhomogeneous airway constriction at the airway opening. *J Appl Physiol* 82: 1349-1359, 1997.

60.   **Thammanomai A, Majumdar A, Bartolak-Suki E, and Suki B**. Effects of reduced tidal volume ventilation on pulmonary function in mice before and after acute lung injury. *J Appl Physiol* 00006.02007, 2007.

61.   **The ARDS Clinical Trials Network, and National Heart Lung and Blood Institute of the National Institute of Health**. Effects of recruitment maneuvers in patients with acute lung injury and acute respiratory distress syndrome ventilated with high positive end-expiratory pressure. *Journal of Critical Care Medicine* 31: 2592-2597, 2003.

62.   **Thompson BT, Hayden D, Matthay MA, Brower R, and Parsons PE**. Clinicians' Approaches to Mechanical Ventilation in Acute Lung Injury and ARDS. *Chest* 120: 1622-1627, 2001.

63.   **Ware LB, and Matthay MA**. The Acute Respiratory Distress Syndrome. *New England Jounral of Medicine* 342: 1334-1349, 2000.

64.   **Weibel E, and Gomez DM, ;**. Architecture of the human lung. *Science* 137: 577-582, 1962.

65.   **Yalcin HC, Perry SF, and Ghadiali SN**. Influence of airway diameter and cell confluence on epithelial cell injury in an in vitro model of airway reopening. *J Appl Physiol* 103: 1796-1807, 2007.

66.   **Yap DY, Liebkemann WD, Solway J, and Gaver DP, 3rd**. Influences of parenchymal tethering on the reopening of closed pulmonary airways. *J Appl Physiol* 76: 2095-2105, 1994.

Appendices

A.1   Nomenclature Table

A.2   Table of Invariant Model/Simulation Parameters

A.3   Analytic Model of Airway Reopening

A.4   Sample Code for Computational Model

A.1: Nomenclature Table

$AIC_{C,M}$: Akaike Information Criterion for model M

$\Delta\left(AIC_{C,M}\right)$: difference between AIC_C scores for model M and the minimum AIC_C

ALI: Acute Lung Injury

Ca : Capillary Number (ratio of viscous to surface tension effects $Ca = \mu v / \gamma$)

E: Model effective lung elastance estimated by fitting single compartment model

E_L : Effective lung elastance computed from recruitment

E_{gas}: Elastic modulus of gas compression in ventilator cylinder

E_{unit} : Elastance of an individual lung unit

H : Elastance from the constant phase model (Experimenal Elastance)

I: Inertia of gas acceleration

j : Unit Imaginary Number

K : Number of elastance measurements

L: Length of the parameter vector

L_θ: Length of the parameter vector, θ

$\min\left\{AIC_{C,j}\right\}$: Model with the minimum $AIC_{C,M}$ score

N: number of airways

N_{open} : Number of open airways

$P\left(\Phi_M \middle| D\right)$ = Probability that model M is correct out of tested models, given the data.

P_0 : Equilibrium pressure of the respiratory system in the chest wall.

$P_{aw}(t)$: Airway Pressure

P_{crit}: Airway critical pressure in original Bates and Irvin model

P_c : Airway critical closing pressure

Pc_μ : Mean of the closing pressure distribution

Pc_σ : Standard deviation of the closing pressure distribution

P_{gas}: Pressure generated by gas compression in the ventilator cylinder

P_o : Airway critical opening pressure

ΔP : Distance between closing and opening pressures.

PEEP: Positive End Expiratory Pressure

r : radius of an airway

R: Model effective lung resistance estimated by fitting single compartment model

R_{eq} : Internal resistance of ventilator tubing and tracheal cannula

R_L : Effective lung resistance computed from recruitment

R_{unit} : Resistance of an individual lung unit

R/D: Recruitment/Derecruitment

S: Grid size, in points per parameter

$S_i = $ Sensitivity of a model to parameter i, ($\partial\Phi/\partial\theta_i$)

S_c : Airway closing velocity constant

s_c : Hyperbolic shape constant for closing velocity distribution

S_o : Airway opening velocity constant

s_o : Hyperbolic shape constant for opening velocity distribution

SSR: Sum of squared residuals between a given model fit and the data

T : Computational time

T_o: is the duration of one iteration

t : Time

Δt : Time step

v: Fluid velocity

V_{cyl} : Volume displaced by the ventilator cylinder

V_{gas} : Volume of gas lost to compression not entering the respiratory system

$V_L(t)$: Lung Volume at time t

$\dot{V}_L(t)$: Flow into or out of the lung at time t

V_T: Ventilator Tidal Volume

$V = A - Be^{-KP_{aw}}$: Salazar and Knowles Equation (A,B,K empirical constants)

x : Airway position on virtual trajectory determining Schmitt Trigger gating

Z_L : Impedence of the Lung

Z_{ti} : Impedence of constant phase tissue elements

α : Constant Phase Model Tissue Hysteresistivity Exponent ($\alpha = \frac{2}{\pi}\tan^{-1}(\eta^{-1})$)

ε_c: Critical Thin film thickness for airway collapse

γ : Surface Tension

Γ : Airway patency of model

η : Hysteresistivity of Constant Phase Model

μ : Viscosity of airway lining fluid

Φ_0 : Error at function minimum in sensitivity analysis

Φ_M : Root mean square error between model M and experiment

Φ_P : Error following perturbation in sensitivity analysis

ω : Frequency of Respiratory Oscillations

θ: Vector of parameter values

θ_0 : Parameter value at function minimum in sensitivity analysis

θ_P : Parameter value after perturbation in sensitivity analysis

A.2: Table of Simulation Parameters

All values presented are stored in the params.m file

Regular Ventilation Parameters	
Dt	.0166666666
Period	.3333
Breaths / Interval	45
Seconds / Interval	15
Tidal Volume	25 ml

Deep Inflation Parameters	
Dt	.005
Period	2
Breaths / Interval	2
Peak Pressure	30 cmH2O

Model Mechanical Parameters	
Number of paths	1250
Open Lung E_L	22 cmH_2O/mL
Open Lung R_L	2 cmH_2O*s/mL
Egas	185 cmH_2O/mL
Rtube	0.41 cmH_2O*s/mL

A.3: Analytic Model of Airway Opening

A simple analytical treatment of reopening behavior in flooded, uncollapsed airways underscores the importance of surfactant in determining meniscus stability in the pulmonary airways. We begun by examining a rigid, cylindrical tube containing two immiscible fluids, one in the liquid and one in the gas phase.

Diagram of the simplified airway model used
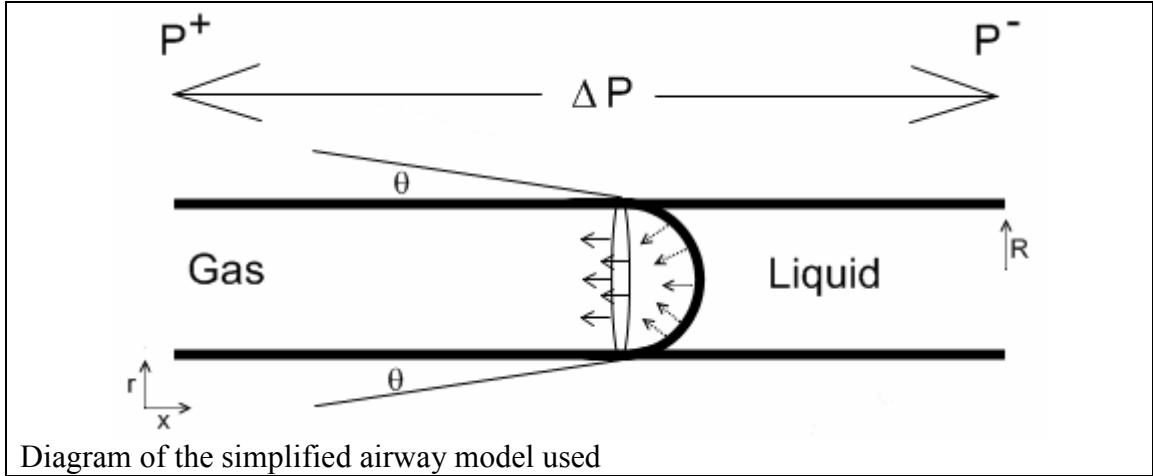
Balancing the fluid and surface stresses in the normal direction at an interface of arbitrary geometry gives us

$$\mathbf{n} \cdot \mathbf{T} \cdot \mathbf{n} = \gamma (\nabla \cdot \mathbf{n})$$

where $\mathbf{n}$ is the unit vector normal to the surface, γ is the surface tension of the interface and $\mathbf{T}$ is the fluid stress tensor. This stress tensor contains the contributions due to both pressure stresses and fluid shear stresses

$$\mathbf{T} = -P\mathbf{I} + \mu \left[\nabla \mathbf{u} + (\nabla \mathbf{u})^T \right]$$

where P is the pressure, $\mathbf{I}$ is the identity matrix, μ is the viscosity and $\mathbf{u}$ is the velocity vector. The force balance on the meniscus then gives the relationship

$$0 = \int_A \nabla P dA - \int_S \left[\gamma (\nabla \cdot \mathbf{n}) - \nabla \cdot (\mu \nabla \mathbf{u}) \right] dS$$

Noting that the normal shear stress, τ, is produced when the meniscus is moving and is proportional to the x-velocity gradient in the radial direction, we obtain

$$\tau_{rx} = -\mu \frac{\partial u_x}{\partial r}$$

as the only pertinent stress in our analysis. Integration over the domain of our geometry and rearranging gives the following relationship for the interfacial force balance

$$\Delta P\left(\pi r^2\right) = \gamma\left(2\pi r\right)\cos(\theta) + \tau_{wall}\left(2\pi r\right)\cos(\theta)$$

where τ_{wall} is the shear stress of the fluid contacting the wall at the interface and θ is the contact angle between the fluid and the wall.

We have used these equations to estimate the required opening pressure for a specific limiting case of this problem and discussed the implications of geometry, contact angle and moving menisci on our estimates. We have assumed that collapse occurs in airways with a radius of approximately 0.1 mm and a surface tension, γ, of 35 dyn/cm. For a static interface, $\tau_{wall} = 0$ as there exists no velocity gradient within the fluid. We have assumed the meniscus to be hemispherical with a contact angle of 0 radians as this configuration generally minimizes the Gibbs free energy of the interface. Additionally, this provides an estimate of the maximal stress at the limiting case of this geometry. Examining this case of a static meniscus reduces the equations to

$$\Delta P = \gamma\left(\frac{2}{r}\right) = \left(35 \times 10^{-3}\ \text{N m}^{-1}\right)\left(\frac{2}{10^{-4}\ \text{m}}\right) = \left(\frac{7 \times 10^{-2}\ \text{N}}{10^{-4}\ \text{m}^2}\right) = \left(700\ \text{N m}^{-1}\right)$$

$$\Delta P = \left(700\ \text{N m}^{-1}\right) \times \left(\frac{1\ \text{cmH}_2\text{O}}{98.0665\ \text{N/m}^2}\right) = 7\ \text{cmH}_2\text{O}$$

which is of similar order to our model's parameter estimates for opening pressures (4.0 cm H_2O in healthy mice to 8.0 cm H_2O in the lung injured mice). Several factors may be

examined that effect the value of this estimate. In the case of a moving meniscus, the pressure required to disrupt the air-liquid interface is higher due to the addition of shear stresse. The impact of viscous effects versus surface tension effects may be assessed by evaluating the capillary number assuming a meniscus velocity, U, of 1 cm/s and a viscosity approximately equal to that of water

$$Ca = \frac{\mu U}{\sigma} \approx \frac{\left(6.82 \times 10^{-4} \text{ Pa s}^{-1}\right)\left(10^{-2} \text{ m s}^{-1}\right)}{35 \times 10^{-3} \text{ N m}^{-1}} = 2.00 \times 10^{-4}.$$

Such a small capillary number in this regime indicates that the surface tension dominates viscous forces; however, decreases in surface tension or increases in either fluid viscosity or velocity would result in an increased importance of the viscous contribution to interfacial stresses.

A.4: Sample Code for Computational Model

The sample code provided consists of the m-files to fit the model to each of the individual mouse elastance time courses from the injured mice. Several variants of the basic program structure were used depending on the precise fitting exercise being performed (ie. Different file names and dimensions for fitting on individual vs. average data). Since the code is preserved with only minor changes between exercises we have chosen to include one example from each archetype of function used in the modeling.

The following files are included:

- minimize_Edif - This function imports the experimental data, determines initial guesses, and calls the optimization routine, stores the optimal parameter values and elastance data to disc, plots the data and calls the sensitivity analysis subroutine.
- model_compare_elast – This function contains all information to run one iteration of the model by initializing parameters, calling the appropriate subfunctions (e.g. ventcycle) to match the ventilator protocol and outputting the error between one model iteration and the experimental data. (elast_fit_plot performs the same computations, however it also graphically displays the elastance data and percentage of open lung as a function of time)
- ventcycle – Performs the actual 15 second ventilation operation and calls REfit_nlin2 to determine effective EL from the model. Functions "Initalize_model.m" and "DI.m" use the same structure, but different parameters with no estimation of EL.
- sens_analysis – Performs sensitivity analysis on the model parameters given their optimal values and the residual error at that point.
- calc_stats.m – Calculates statistics on each optimal parameter.
- REfit_nlin2 – Performs non-linear regression to estimate the values of EL and RL from the Pressure, Volume and Flow tracings generated by the model over 4 breaths.

Not included in this appendix are any stand-alone functions explicitly for plotting data, generating new random number draws or other more trivial tasks.

```
% minimize_Edif  - imports experimental data, determines initial
guesses, calls optimization routine, stores the optimal parameter
values and elastance data to disc, plots the data and calls the
sensitivity analysis subroutine.

tic
format long
% Initalize variables and set optimization tolerances/parameters
options = OPTIMSET('display','iter','TolX',5e-5,'TolFun',5e-
5,'MaxFunEvals',350);
[dt, period, cycles, tmax, measures, n_paths,  Eunit, Runit, Egas,
Rtube, RL, EL, IE, A, DI_dt, DI_period, DI_cycles, DI_tmax] = params();
global Exp_data;
global Exp_time;
```

```
global X;
global collumnbank

% Specify Lognormal Distribution or Plotting?
ln_on = 2;
ploton = 0;
gen_new_rands(n_paths,ln_on)        %Generate new Random Numbers

slopes  = dlmread('slopes.txt');    %Import Opening Slopes
slopes2 = dlmread('slopes2.txt');   %Import Closing Slopes

%Choose Appropriate Pressure Distribution
if ln_on == 1
    presses = dlmread('Pc.txt');
else
    presses = dlmread('Pressures.txt');
end

% Import Experimental Data
ALI_data = dlmread('Injured_individual_data.csv',',',1,0);
Exp_time = ALI_data(:,1);

% Generate Matrix of Initial Guesses
Xbank = [-0.078563      5.6436      0.024601    0.0042108   3.5219;
         -0.039985      4.5028      0.034730    0.0049404   3.7645;
         -0.041435      3.0645      0.031707    0.005457    4.4315;
           0.1969   3.9027         0.045241    0.0054051   5.2364;
           2.7833   2.8755         0.040509    0.0039209   3.5460;
           3.1468   2.6506         0.037368    0.0047305   3.5201;
           4.0768   3.6492         0.025666    0.0044427   3.4470;
           4.2990   3.7432         0.024261    0.0048129   3.3983];

% Initalize Variables
collumnbank = [2:10, 12:19, 21:28, 29:37];
num_sims = length(collumnbank);
Pc_mean  = zeros(1,num_sims);
Pc_std   = zeros(1,num_sims);
Po_mean  = zeros(1,num_sims);
Po_std   = zeros(1,num_sims);
xstore   = zeros(num_sims,5);
rmsstore = zeros(1,num_sims);
Elog     = zeros(num_sims,length(Exp_time));
Openlog  = zeros(num_sims,length(Exp_time));

start = 2;
term = num_sims;
% Begin Fitting Model to all Data (Start to Term)
for j = start:term;
    collumn = collumnbank(j);
    Exp_data = ALI_data(:,collumn);
    clear f_temp

    % Test each potential starting X to find best initial guess.
    for k = 1:8;
        X = Xbank(k,1:5);
```

86

```matlab
        [Ejunk,Ojunk,f_temp(k-4)] = elast_fit_plot(X,0);
    end
    [val,I] = min(f_temp(:));
    X = Xbank(I+4,:);

    % Use Nelder + Mead Simplex Search to minimize model_compare_elast
    [xstore(j,:),rmsstore(j),exitflag] =
fminsearch(@model_compare_elast, X,options);

end

% Estimate critical Pressure distribution characteristics + plot output
for j = start:term;

    collumn = collumnbank(j);
    Exp_data = ALI_data(:,collumn);

    [Elog(j,:),Openlog(j,:),R(j,:)] = elast_fit_plot(xstore(j,:),1);

if ln_on == 1
[Pc_mean(j),Pc_std(j),Po_mean(j),Po_std(j)]=lnplot(xstore(j,1),xstore(j
,2),xstore(j,5))
else

Pc_dist(j,1:n_paths) = xstore(j,1) + xstore(j,2)*presses;
Po_dist(j,1:n_paths) = xstore(j,1) + xstore(j,2)*presses + xstore(j,5);
Pc_mean(j) = mean(Pc_dist(j,:));
Po_mean(j) = mean(Po_dist(j,:));
Pc_std(j) = std(Pc_dist(j,:));
Po_std(j) = std(Po_dist(j,:));

    end
end

% Store Data To Disc
start = 1; term=length(collumnbank);
p_span(start:term) =
100*rmsstore(start:term)./(max(Elog(start:term,:)') -
min(Elog(start:term,:)'));
A = [xstore(start:term,1:2)'; Pc_mean(start:term); Pc_std(start:term);
Po_mean(start:term);
Po_std(start:term);xstore(start:term,3:5)';rmsstore(start:term);p_span(
start:term)];
B = [Exp_time,Elog(start:term,:)'];
C = [0,collumnbank(1:term);B];
dlmwrite('model_fit.csv',A);
dlmwrite('model_output.csv',C);

% Begin Plotting Routines
Econtrol = mean(Elog(1:4,:));
Datacontrol = mean(ALI_data(:,2:5)');
Data = [Datacontrol;ALI_data(:,7:10)'];
figure(),
hold on;
plot(Exp_time,[Econtrol;Elog(5:8,:)]);plot(Exp_time(:),Data(:,:)','.')
```

```
xlabel('Time (s)')
ylabel('Elastance cmH20*s^2/L')
legend('Control','4 Hours','14 Hours', '24 Hours', '48 Hours')

% Perform Sensitivity Analysis
[plus_sens,minus_sens,plus_err,minus_err] =
sens_analysis(xstore,rmsstore)
```

```
function [RMSR] = model_compare_elast(parameters);

% model_compare_elast(parameters) takes the 5 parameters from the R/D
model
% and uses them to compute an elastance time course, which it
% compares to the experimental data in the column numbered 'column' of
% ALI_data.  This function contains all information to run one
iteration of the % model by initializing parameters, calling the
appropriate subfunctions (e.g.
% ventcycle) to match the ventilator protocol and outputting the error
between
% one model iteration and the experimental data.

global Exp_data;
global Exp_time;

kmax = 3;
mmax = 25;

% Initalize Constant Variables
[dt, period, cycles, tmax, measures, n_paths, Eunit, Runit, Egas,
Rtube, RL, EL, IE, A, DI_dt, DI_period, DI_cycles, DI_tmax] = params();
Esample = zeros(kmax,mmax);
Opensample = zeros(kmax,mmax);
Emag = zeros(kmax,mmax);
%masterE = zeros(1,length(1 + (kmax-1).k.*mmax));
%masteropen = zeros(1,length(1 + (kmax-1).*mmax:k.*mmax));

PEEP_list = [1,3,6];

slopes = dlmread('slopes.txt')';
slopes2 = dlmread('slopes2.txt')';
pressures = dlmread('Pressures.txt')';

% Assign parameters
Pc_mu = parameters(1);
Pc_sd = parameters(2);
so = parameters(3);
sc = parameters(4);
delta_P = parameters(5);

% Generate distributions of R/D parameters.
Pcrit = zeros(1,n_paths);
So = zeros(1,n_paths);
Sc = zeros(1,n_paths);
Pcrit(:)  = Pc_mu + pressures.*Pc_sd;
```

```
So(:)    = so./slopes;
Sc(:)    = sc./slopes2;

R = zeros(1,measures);
E = zeros(1,measures);
Pc0 = zeros(1,measures);
VL0 = zeros(1,measures);
VLdot0 = zeros(1,measures);
V0 = zeros(1,measures);
Vdot0 = zeros(1,measures);
X0 = zeros(1,measures);
Xstate0 = zeros(1,measures);

%  Initalize model from closed state
PEEP = PEEP_list(1);
m = 1;
[Pcint,VLint,VLdotint,Vint, Vdotint,Xint, Xstateint, R, E] =
initalize_model(Pcrit, So, Sc, delta_P,PEEP);

% Begin ventilation at each PEEP, cycle through protocol
for k = 1:kmax;

    PEEP = PEEP_list(k);
    [Pc0,VL0,VLdot0,V0, Vdot0,X0, Xstate0, R,E,open] =
ventcycle(Pcint,VLint,VLdotint,Vint, Vdotint,Xint, Xstateint, R,E,
Pcrit, So, Sc,delta_P, PEEP);
    [Pc0,VL0,VLdot0,V0, Vdot0,X0, Xstate0, R,E,open] =
ventcycle(Pc0,VL0,VLdot0,V0,Vdot0,X0,Xstate0,R,E,Pcrit, So,
Sc,delta_P,PEEP);
    [Pc0,VL0,VLdot0,V0, Vdot0,X0, Xstate0, R,E,open] =
DI(Pc0,VL0,VLdot0,V0,Vdot0,X0,Xstate0,R,E,Pcrit, So, Sc,delta_P,PEEP);

    mc(1) = 1;
    Etrend(1) = E;
    Rtrend(1) = R;
    opentrend(1) = open;

    for m = 1:20;
        [Pc0,VL0,VLdot0,V0, Vdot0,X0, Xstate0, R,E,open] =
ventcycle(Pc0,VL0,VLdot0,V0,Vdot0,X0,Xstate0,R,E,Pcrit, So,
Sc,delta_P,PEEP);
        mc(m) = m;
        Etrend(m) = E;
        Rtrend(m) = R;
        opentrend(m) = open;
    end

    for m = 21:mmax
        [Pc0,VL0,VLdot0,V0, Vdot0,X0, Xstate0, R,E,open] =
ventcycle(Pc0,VL0,VLdot0,V0,Vdot0,X0,Xstate0,R,E,Pcrit, So,
Sc,delta_P,PEEP);
        [Pc0,VL0,VLdot0,V0, Vdot0,X0, Xstate0, R,E,open] =
ventcycle(Pc0,VL0,VLdot0,V0,Vdot0,X0,Xstate0,R,E,Pcrit, So,
Sc,delta_P,PEEP);
        mc(m) = m;
```

```
        Etrend(m) = E;
        Rtrend(m) = R;
        opentrend(m) = open;
    end

    % Store elastance and fractional opening information
    Esample(k,:) = Etrend(:);
    Opensample(k,:) = opentrend(:);
    masterE(1 + (k-1).*mmax:k.*mmax) = Esample(k,:)';
    masteropen(1 + (k-1).*mmax:k.*mmax) = Opensample(k,:)';
end

%Compute Residual Error
SSR = sum((Exp_data(:) - masterE(:)).^2);
% Display parameter values and RMS Error.
[parameters]
RMSR = [sqrt(SSR/75)]
```

```
function [Pcint,VLint,VLdotint,Vint, Vdotint,Xint,Xstateint, R, E,
open] = ventcycle(Pcint,VLint,VLdotint,Vint, Vdotint,Xint, Xstateint,
R,E, Pcrit, So, Sc,delta_P,PEEP,deltavect);
plotson = 0;
[dt, period, cycles, tmax, measures, n_paths,  Eunit, Runit, Egas,
Rtube, RL, EL, IE, A, DI_dt, DI_period, DI_cycles, DI_tmax] = params();
% disp('Experimental Breaths')
time = zeros(1,ceil((cycles*tmax)));
Vcyl = zeros(1,ceil((cycles*tmax)));
Vgas = zeros(1,ceil((cycles*tmax)));
Pc = zeros(1,ceil((cycles*tmax)));
V = zeros(n_paths,ceil((cycles*tmax)));
VL = zeros(1,ceil((cycles*tmax)));
Vdot = zeros(n_paths,ceil((cycles*tmax)));
VLdot = zeros(1,ceil((cycles*tmax)));
Pgas = zeros(1,ceil((cycles*tmax)));
n_open = zeros(1,ceil((cycles*tmax)));
x = zeros(n_paths,ceil((cycles*tmax)));
avg_x = zeros(1,ceil((cycles*tmax)));
xstate = zeros(n_paths,ceil((cycles*tmax)));
DV = zeros(1,ceil((cycles*tmax)));

for m = 1:measures
breath = 0;

        %Carry over current model state to next measurement course
        VL(1) = VLint;
        Pc(1) = Pcint;
        Vcyl(1) = 0;
        VLdot(1) = VLdotint;
        V(:,1) = Vint;
        Vdot(:,1) = Vdotint;
        x(:,1) = Xint;
        xstate(:,1) = Xstateint;
        R = RL;
```

```matlab
        E = EL;

    % Enter loop to control ventilation and paramater estimation
    for t = 2:ceil(cycles*tmax);
        time(t) = t.*dt;            % Keep

        Vcyl(t)  = A.*.05*abs(sin(pi.*(t)/(tmax)));
        % Cycle between piston and peep for IE ratio of 1:1
        if Vcyl(t) < Vcyl(t-1); %mod(t,tmax/2) == 0;
            IE = 1;
        else
            IE = 0;
        end

         if IE == 1
             % Exhale Passively against PEEP
             Vgas(t)  = 0;
             Pgas(t)  = 0;
             Pc(t)    = PEEP + (Rtube/(Rtube+RL))*(VL(t-1).*EL - PEEP);
          elseif  IE == 0;

             Vgas(t)  = Vgas(t-1) + (Vcyl(t) - Vcyl(t-1)) - (Pc(t-1) -
VL(t-1)*EL)*dt/(Rtube + RL) ;
             Pgas(t)  = Egas*Vgas(t);
             Pc(t) = Pgas(t) - (Rtube/(RL))*((Pc(t-1) - VL(t-1).*EL));

          else
          end

        %
        n_open(t) = 0;              % Zero out number of open lung units

        % Cycle through individual flow pathways
        for i = 1:n_paths

            % Determine opening velocity of airway i at time t
            if Pc(t) > Pcrit(i) + delta_P;
            x(i,t) = x(i,t-1) + So(i).*(Pc(t) - Pcrit(i) - delta_P)*dt;
            elseif Pc(t) < Pcrit(i);
                x(i,t) = x(i,t-1) - Sc(i).*(Pcrit(i) - Pc(t))*dt;
            else
                x(i,t) = x(i,t-1);
            end

    % Determine if airway transitions between open/closed state and
    % track number of presently open airways
            if x(i,t) <= 0;
                x(i,t) = 0;
                xstate(i,t) = 0;
            elseif x(i,t) >= 1;
                x(i,t) = 1;
                xstate(i,t) = 1;
                n_open(t) = n_open(t) + 1;
            else
                xstate(i,t) = xstate(i,t-1);
```

```
                if xstate(i,t) == 1;
                    n_open(t) = n_open(t) + 1;
                else
                end
            end

    % Determine flow and volume in airway i at time t
            if xstate(i,t) == 1;
                Vdot(i,t)  = (1/Runit)*(Pc(t) - V(i,t-1)*Eunit);
                V(i,t) = V(i,t-1) + Vdot(i,t)*dt;
    % Add total lung volume and flow resulting from airway i at time t
                VLdot(t) = VLdot(t) + Vdot(i,t);
                VL(t)  = VL(t) + V(i,t);
            else
                V(i,t) = V(i,t-1);
            end
        end

        if n_open(t) == 0;
            RL = Runit;
            EL = Eunit;
        else
            RL = Runit./n_open(t);
            EL = Eunit./n_open(t);
        end
    end

if m == measures
    % Estimate values of R,E from plots;
    [E,R,SSR] = REfit_nlin2(VL, VLdot, Pc, EL,RL, t, time, tmax);
    open = sum(Xstateint);
else
end

if plotson == 1
ventplot(time,Pc,VL,VLdot)
    %if m >= 5
        figure,hold on
        plot(time(:),sum(xstate,1)/n_paths)
        title('Number of open paths')
    %else
    %end

    if m >= 1000;%mmax;
% show recruitment: Vdot,V,airway_start,airway_end,start,end,tmax)
        recruit_plot3d(Vdot,V,1,40,1,3,tmax);
    else
    end

else
end

    VLint     = VL(t);
    Pcint     = Pc(t);
    Vcylint   = 0;
```

```
    VLdotint  = VLdot(t);
    Vint      = V(:,t);
    Vdotint   = Vdot(:,t);
    Xint      = x(:,t);
    Xstateint = xstate(:,t);

if m < measures;
    Pc = zeros(1,ceil((cycles*tmax)));
    V = zeros(n_paths,ceil((cycles*tmax)));
    VL = zeros(1,ceil((cycles*tmax)));
    Vdot = zeros(n_paths,ceil((cycles*tmax)));
    VLdot = zeros(1,ceil((cycles*tmax)));

    %Carry over current model state to next measurement course
    VL(1) = VLint;
    Pc(1) = Pcint;
    Vcyl(1) = 0;
    VLdot(1) = VLdotint;
    V(:,1) = Vint;
    Vdot(:,1) = Vdotint;
    x(:,1) = Xint;
    xstate(:,1) = Xstateint;
    R = RL;
    E = EL;
    open = sum(Xstateint);

else
end
end
```

```
% function [plus_sens,minus_sens,plus_err,minus_err] =
sens_analysis(xstore,rmsstore)
% Sensitivity Analysis
% clear Xtrend, clear error_p, clear error_n
%Initalize / Globalize Variables
[dt, period, cycles, tmax, measures, n_paths,  Eunit, Runit, Egas,
Rtube, RL, EL, IE, A, DI_dt, DI_period, DI_cycles, DI_tmax] = params();
global Exp_data;
global Exp_time;
global X;
global collumnbank

% Import Distributions, Experimental Data & Parameters
slopes  = dlmread('slopes_health.txt');
slopes2 = dlmread('slopes2_health.txt');
presses = dlmread('Pressures_health.txt');
ALI_data = dlmread('Healthy_individual_data.csv',',',2,0);
Exp_time = ALI_data(:,1);
Parameter_sets = dlmread('Healthy model_fit.csv',',',0,0);
xstore = Parameter_sets([1,2,7,8,9],:)';
rmsstore = Parameter_sets(10,:)';
Healthy_margs = [1,5; 6,10; 11,15; 16,20;];
Healthy_sims =  [1:5, 6:10, 11:15, 16:20];
```

```
collumnbank = [2:6, 8:12, 14:18, 20:24];

L = length(collumnbank)                    % number of data sets imported
P = 5;                                      % number of Parameters

Pbank = [.25, .5, 1];           % Pc Increment

m = 1;
%Scroll through experimental data set
for i = 1:L
    collumn = collumnbank(i);
    Exp_data = ALI_data(:,collumn);
    sim_num = Healthy_sims(i)

    k = 1;                 % Handle Pc Differently
    Xi = xstore(i,:);

    %  Compute sensitivity in positive direction
    Xi(k) = xstore(k) + Pbank(m);
    error_p(i,k) = model_compare_elast(Xi);
    plus_sens(i,k) = (Xi(k) - xstore(i,k) )./(xstore(i,k));;
    plus_err(i,k) = (rmsstore(i) - error_p(i,k))/rmsstore(i);

    %  Compute sensitivity in negative direction
    Xi(k) = xstore(k) - Pbank(m);
    error_n(i,k) = model_compare_elast(Xi);
    minus_sens(i,k) = (Xi(k) - xstore(i,k) )./(xstore(i,k));;
    minus_err(i,k) = (rmsstore(i) - error_n(i,k))/rmsstore(i);

    %  Scroll through other 4 parameters and record sensitivity
    for k = 2:P;

        ik = [i     k    ]

        Xi = xstore(i,:);
        Xi(k) = .95*Xi(k);
        Xtrend_n(i,k) = Xi(k);
        error_n(i,k) = model_compare_elast(Xi);
        minus_sens(i,k) = (Xi(k) - xstore(i,k) )./(xstore(i,k));;
        minus_err(i,k) = (rmsstore(i) - error_n(i,k))/rmsstore(i);


        Xi = xstore(i,:);
        Xi(k) = 1.05*Xi(k);
        Xtrend_p(i,k) = Xi(k);
        error_p(i,k) = model_compare_elast(Xi);
        plus_sens(i,k) = (Xi(k) - xstore(i,k) )./(xstore(i,k));;
        plus_err(i,k) = (rmsstore(i) - error_p(i,k))/rmsstore(i);

    end

end

dE_dX_plus(1:L,:)  = plus_err(1:L,:)./plus_sens(1:L,:);
dE_dX_minus(1:L,:) = minus_err(1:L,:)./minus_sens(1:L,:);
```

```
plus_output = plus_err(1:L,:);
minus_output = minus_err(1:L,:);

dlmwrite('plus_output_health.csv',plus_output,',')
dlmwrite('minus_output_health.csv',minus_output,',')

margs = Healthy_margs;

for i = 1:4;
  avgplus_health(i,:) = mean( plus_output(margs(i,1):margs(i,2),:) );
  avgminus_health(i,:) = mean( minus_output(margs(i,1):margs(i,2),:) );
  stdplus_health(i,:) = std( plus_output(margs(i,1):margs(i,2),:) );
  stdminus_health(i,:) = std( minus_output(margs(i,1):margs(i,2),:) );
  avg_dE_dX_plus_health(i,:) = mean(
dE_dX_plus(margs(i,1):margs(i,2),:) );
  avg_dE_dX_minus_health(i,:) = mean(
dE_dX_minus(margs(i,1):margs(i,2),:) );
  std_dE_dX_plus_health(i,:)=std(dE_dX_plus(margs(i,1):margs(i,2),:));
  std_dE_dX_minus_health(i,:) = std(
dE_dX_minus(margs(i,1):margs(i,2),:) );
end

dlmwrite('avg_plus_health.csv',avgplus_health,',')
dlmwrite('avg_minus_health.csv',avgminus_health,',')
dlmwrite('std_plus_health.csv',stdplus_health,',')
dlmwrite('std_minus_health.csv',stdminus_health,',')

dlmwrite('avg_dE_dX_plus_health.csv',avg_dE_dX_plus_health,',')
dlmwrite('avg_dE_dX_minus_health.csv',avg_dE_dX_minus_health,',')
dlmwrite('std_dE_dX_plus_health.csv',std_dE_dX_plus_health,',')
dlmwrite('std_dE_dX_minus_health.csv',std_dE_dX_minus_health,',')
%%%%%%%%%%%%%%%%%%%%%%%%%%%%%%%%%%%%%%%%%%%%%%%%%%%%%%%%%%%%%%%%%%%%%%
%%%  Code Below Ommitted, Identical content on Injured Data Sets.  %%%
%%%%%%%%%%%%%%%%%%%%%%%%%%%%%%%%%%%%%%%%%%%%%%%%%%%%%%%%%%%%%%%%%%%%%%
```

```
%  calc_stats.m  - Calculates mean and standard deviations on each
% parameter for each individual animal.  Current Configuration for
% Injured data only.  Identical code exists for Healthy mice.

% Initalize, Globalize Variables + Import Data
global Exp_data;
global Exp_time;
global X;
ALI_data = dlmread('ALI_data.csv',',',1,0);
Exp_time = ALI_data(:,1);
ALIbank = [7:10];
Elog = dlmread('model_output.csv',',',1,0);
Elog = Elog';
A = dlmread('model_fit.csv');

% Set margins and dimensions from data
margs = [1,9; 10,17; 18,25; 27,34];
dim_a = size(A);
```

95

```matlab
% Cycle through 4 time conditions (4,14,24,48 hrs)
for i = 1:4;
    head = margs(i,1);  % Beginning column of data for time point
    tail = margs(i,2);  % Final column of data for time point

    for j = 1:dim_a(1)        % Cycle through parameters)
        averages(j,i) = mean(A(j,head:tail));   % Average parameters
        stds(j,i)     = std(A(j,head:tail));    % parameters Std dev.

    end

    % Shift by one to match column labels to elastance tracings
    head = head+1;
    tail = tail+1;

    % Compute Average and std.dev of E(t) for each condition
    averageE(i,:) = mean(Elog(head:tail,:));
    stdevE(i,:)   = std(Elog(head:tail,:));

    collumn = ALIbank(i);
    Exp_data = ALI_data(:,collumn);

    % Plot Average model E with Average Experimental elastance
    figure()
    plot(Exp_time(:),Exp_data(:),'b.',Exp_time(:),averageE(i,:),'r-
',Exp_time(:),(averageE(i,:) + stdevE(i,:)/sqrt(margs(i,2)-
margs(i,1)+1)),'r--',Exp_time(:),(averageE(i,:) -
stdevE(i,:)/sqrt(margs(i,2)-margs(i,1)+1)),'r--')
        xlabel('Time (s)')
        ylabel('Elastance cmH20*s^2/L')

% Compute error between average model and average experiment
MSQR(i) = sqrt(sum((Exp_data(:) - averageE(i,:)').^2)/75);
end

CVs = stds./averages;   %Coefficient of Variation for each Parameter

%Write Parameter Stats
dlmwrite('averages.csv',averages);
dlmwrite('stds.csv',stds);
dlmwrite('CVs.csv',CVs);

CVE = stdevE./averageE; %Coefficient of Variation for each Elastance

%Write Elastance Stats
dlmwrite('averageE.csv',averageE);
dlmwrite('stdevE.csv',stdevE);
dlmwrite('CVE.csv',CVE);

% Create matrix of average parameters
xstore_t = [averages(1:2,:); averages(7:9,:)];

% Scroll through each condition, plotting model evaluated at average
% parameter value with average elastance.
for j = 1:4;
```

```
    collumn = ALI_bank(j);
    % Exp_data = AVG_data(:,collumn);

    [Elog_t(j,:),Openlog_t(j,:),R_t(j,:)] =
elast_fit_plot(xstore_t(:,j),1);
end
```

```
function [E,R,resnorm] = REfit_nlin2(VL, VLdot, Pc, EL,RL, t, time,
tmax);

% Truncate Data to 4 breaths
    t = round(t-1);
    tmax = round(tmax);
    Xdata = [VL(t-4*tmax:t)' , VLdot(t-4*tmax:t)'];
    Ydata = Pc((t-4*tmax:t))';

x0 = [EL; RL];    % Vectorized initial guess
options = optimset('TolFun',1e-8,'Tolx',1e-8);  % Set options

%Minimize fun (two compartment model) using least squares curve fit
fun = @(x,xdata) x(1).*xdata(:,1) + x(2).*xdata(:,2);
[PARS,resnorm] = lsqcurvefit(fun,x0,Xdata,Ydata,0,1000,options);

E = PARS(1); R = PARS(2);    % Pass E,R
plotson = 0;
if plotson == 1;
% Plot 2-cpt model fit and Actual model pressure
Pnew = Xdata(:,1).*PARS(1) + Xdata(:,2).*PARS(2);

 figure,
 hold on
 plot(time(t-length(Ydata):t), Pc(t-length(Ydata):t),'r-', time(t-
length(Ydata)+1:t), Pnew(:),'b:')
 %plot(Pc(t-length(Ydata):t),'r-')
 %plot(Pnew(:),'b:')
 legend('Actual Pressure Tracing', 'Model Fitting')
 % plot(time(t-length(Ydata):t), (Pnew(:) + abs(residual)) ,'k+',
time(t-tmax:t), (Pnew(:) - abs(residual)), 'k+')
else
end
```